International Tables for Crystallography (2006). Vol. C, Chapter 2.6, pp. 89–112.

2.6. Small-angle techniques

By O. Glatter and R. May

2.6.1. X-ray techniques (By O. Glatter)

2.6.1.1. *Introduction*

The purpose of this section is to introduce small-angle scattering as a method for investigation of nonperiodic systems. It should create an understanding of the crucial points of this method, especially by showing the differences from wide-angle diffraction. The most important concepts will be explained. This article also contains a collection of the most important equations and methods for standard applications. For details and special applications, one must refer to the original literature or to textbooks; the reference list is extensive but, of course, not complete.

The physical principles of scattering are the same for wide-angle diffraction and small-angle X-ray scattering. The electric field of the incoming wave induces dipole oscillations in the atoms. The energy of X-rays is so high that all electrons are excited. The accelerated charges generate secondary waves that add at large distances (far-field approach) to give the overall scattering amplitude. All secondary waves have the same frequency but may have different phases caused by the different path lengths. Owing to the high frequency, it is only possible to detect the scattering intensity – the square of the scattering amplitude – and its dependence on the scattering angle.

The angle-dependent scattering amplitude is related to the electron-density distribution of the scatterer by a Fourier transformation. All this holds for both wide-angle diffraction and small-angle X-ray scattering. The main difference is that in the former we have a periodic arrangement of identical scattering centres (particles), *i.e.* the scattering medium is periodic in all three dimensions with a large number of repetitions, whereas in small-angle scattering these particles, for example proteins, are not ordered periodically. They are embedded with arbitrary orientation and with irregular distances in a matrix, such as water. The scattering centres are limited in size, non-oriented, and nonperiodic, but the number of particles is high and they can be assumed to be identical, as in crystallography.

The Fourier transform of a periodic structure in crystallography (crystal diffraction) corresponds to a Fourier series, *i.e.* a periodic structure is expanded in a periodic function system.

The Fourier transform of a non-periodic limited structure (small-angle scattering) corresponds to a Fourier integral. In mathematical terms, it is the expansion of a nonperiodic function by a periodic function system.

So the differences between crystallography and small-angle scattering are equivalent to the differences between a Fourier series and a Fourier integral. It may seem foolish to expand a non-periodic function with a periodic function system, but this is how scattering works and we do not have any other powerful physical process to study these structures.

The essential effect of these differences is that in small-angle scattering we measure a continuous angle-dependent scattering intensity at discrete points instead of sharp, point-like spots as in crystallography.

Another important point is that in small-angle scattering we have a linear increase of the signal (scattered intensity) with the number of particles in the measuring volume since intensities are adding. Amplitudes are adding in crystallography, so we have a quadratic relation between the signal and the number of particles.

In addition, there is a loss of information in small-angle scattering experiments caused by the averaging over all orientations in space. The three-dimensional structure is represented by a one-dimensional function – the dependence of the scattered intensity on the scattering angle. This is also true for powder diffraction. To recover the structure uniquely is therefore impossible.

The computation of the scattering function for a known structure is called the solution of the scattering problem. This problem can be solved exactly for many different structures. The inversion, *i.e.* the estimation of the structure of the scatterer from its scattering functions, is called the inverse scattering problem. This problem cannot be solved uniquely.

The description and solution of the scattering problem gives information to the experimenter concerning the scattering functions to be expected in a special situation. In addition, this knowledge is the starting point for the evaluation and interpretation of experimental data (solution of the inverse problem).

There are methods that give a rough first-order approximation to the solution of the inverse scattering problem using only a minimum amount of *a priori* information about the system to obtain an initial model. In order to improve this model, one has to solve the scattering problem. The resulting theoretical model functions are compared with the experimental data. If necessary, model modifications are deduced from the deviations. After some iterations, one obtains the final model.

It should be noticed that it is possible to find different models that fit the data within their statistical accuracy. In order to reduce this ambiguity, it is necessary to have additional independent information from other experiments. Incorrect models, however, can be rejected when their scattering functions differ significantly from the experimental data.

What type of investigations can be performed with small-angle scattering? It is possible to study monodisperse and polydisperse systems. In the case of monodisperse systems, it is possible to determine size, shape, and, under certain conditions, the internal structure. Monodispersity cannot be deduced from small-angle scattering data and must therefore be assumed or checked by independent methods.

For polydisperse systems, a size distribution can be evaluated under the assumption of a certain shape for the particles (*particle sizing*).

All these statements are strictly true for highly diluted systems where the interparticle distances are much larger than the particle dimensions. In the case of semi-dilute systems, the result of a small-angle scattering experiment is influenced by the structure of the particles and by their spatial arrangement. Then the scattering curve is the product of the particle scattering function and of the interparticle interference function. If the scattering function of one particle is known, it is possible to evaluate information about the radial distribution of these particles relative to each other. If the system is dense, *i.e.* if the volume fraction of the particles (scattering centres) is of the same order of magnitude as the volume fraction of the matrix, it is possible to determine these volume fractions and a characteristic length of the phases. The most important practical applications, however, pertain to dilute systems.

How are small-angle scattering experiments related to other scattering experiments? Small-angle scattering uses radiation with a wavelength in the range 10^{-1} to 10^{0} nm, depending on the

problem and on the source used. This range is similar for X-rays and neutrons, but neutrons interact with the nuclei of the atoms whereas X-rays interact with the electrons. The scattering efficiency increases linearly with the atomic number for X-rays. The dependence is much more complicated for neutrons and does not show a systematic trend. The essential fact in neutron scattering is the pronounced difference in the scattering power between hydrogen and deuterium, which is important for varying the contrast between the particles and the matrix.

The wavelength and the scattering efficiency limit the range of small-angle scattering experiments to systems in the size range of a few nanometres up to about 100 nm. Special instruments permit the study of larger particles (Bonse & Hart, 1967; Koch, 1988). These instruments need a high intensity of the primary beam (synchrotron radiation) and are not very common.

Particles in the size range from 100 nm up to some micrometres can be investigated by static light-scattering techniques (Glatter, Hofer, Jorde & Eigner, 1985; Glatter & Hofer, 1988*a,b*; Hofer, Schurz & Glatter, 1989). Particles exceeding this limit can be seen in an optical microscope or can be studied with Fraunhofer diffraction (Bayvel & Jones, 1981).

Electron microscopy is in competition with all these scattering methods. It has the marked advantage of giving real pictures with rather high resolution but it has the inherent disadvantage that the preparation may introduce artefacts. Small-angle scattering, on the other hand, is a method to study macromolecules in solution, which is a very important advantage for biological samples and for polymers.

Crystallography gives more information about the particle (atomic structure) and can be applied to relatively large systems. It is possible to study particles as large as proteins and viruses if good crystals of these substances are available. The experiment needs synchrotron radiation for large molecules like proteins or viruses, *i.e.* access to a large research facility is necessary. Small-angle X-ray scattering with conventional generators is a typical next-door technique with the advantage of ready availability.

Small-angle scattering has developed into a standard measuring method during recent decades, being most powerful for the investigation of submicrometre particles.

2.6.1.2. *General principles*

In this subsection, we are concerned with X-rays only, but all equations may also be applied with slight modifications to neutron or electron diffraction. When a wave of X-rays strikes an object, every electron becomes the source of a scattered wave. All these waves have the same intensity given by the Thomson formula

$$I_e(\theta) = I_p T_f \frac{1}{a^2}\frac{1+\cos^2 2\theta}{2}, \qquad (2.6.1.1)$$

where I_p is the primary intensity and a the distance from the object to the detector. The factor T_f is the square of the classical electron radius ($e^2/mc^2 = 7.90 \times 10^{-26}$[cm^2]). The scattering angle 2θ is the angle between the primary beam and the scattered beam. The last term in (2.6.1.1) is the polarization factor and is practically equal to 1 for all problems dealt with in this subsection. I_e should appear in all following equations but will be omitted, *i.e.* the amplitude of the wave scattered by an electron will be taken to be of magnitude 1. I_e is only needed in cases where the absolute intensity is of interest.

The amplitudes differ only by their phases φ, which depend on the positions of the electrons in space. Incoherent (Compton) scattering can be neglected for small-angle X-ray scattering. The phase φ is $2\pi/\lambda$ times the difference between the optical path length of the wave and an arbitrary reference wave (with λ being the wavelength). The direction of the incident beam is defined by the unit vector $\mathbf{s}_0$ and of the scattered beam by $\mathbf{s}$. The angle between these two unit vectors (scattering angle) is 2θ. The path difference between the rays through a point P and an arbitrary origin O is $-\mathbf{r}(\mathbf{s}-\mathbf{s}_0)$. The phase is $\varphi = -\mathbf{h}\cdot\mathbf{r}$ if we define the scattering vector $\mathbf{h}$ as

$$\mathbf{h} = (2\pi/\lambda)(\mathbf{s}-\mathbf{s}_0). \qquad (2.6.1.2)$$

This vector bisects the angle between the scattered beam and the incident beam and has length $h = (4\pi/\lambda)\sin\theta$. We keep in mind that $\sin\theta$ may be replaced by θ in small-angle scattering. We now introduce the electron density $\rho(\mathbf{r})$. This is the number of electrons per unit volume at the position $\mathbf{r}$. A volume element $\mathrm{d}V$ at $\mathbf{r}$ contains $\rho(\mathbf{r})\,\mathrm{d}V$ electrons. The scattering amplitude of the whole irradiated volume V is given by

$$A(\mathbf{h}) = \iiint \rho(\mathbf{r})\exp(-i\mathbf{h}\cdot\mathbf{r})\ \mathrm{d}V. \qquad (2.6.1.3)$$

We see that the amplitude A is the Fourier transform of the electron-density distribution ρ. The intensity $I(\mathbf{h})$ of the complex amplitude $A(\mathbf{h})$ is the absolute square given by the product of the amplitude and its complex conjugate A^*,

$$I(\mathbf{h}) = A(\mathbf{h})A(\mathbf{h})^* = \iiint \widetilde{\rho}^2(\mathbf{r})\exp(-i\mathbf{h}\cdot\mathbf{r})\ \mathrm{d}V, \qquad (2.6.1.4)$$

where $\widetilde{\rho}^2(\mathbf{r})$ is the convolution square (Bracewell, 1986):

$$\widetilde{\rho}^2(\mathbf{r}) = \iiint \rho(\mathbf{r}_1)\rho(\mathbf{r}_1-\mathbf{r})\ \mathrm{d}V_1. \qquad (2.6.1.5)$$

The intensity distribution in $\mathbf{h}$ or reciprocal space is uniquely determined by the structure in real space.

Until now, we have discussed the scattering process of a particle in fixed orientation in vacuum. In most cases of small-angle scattering, the following situation is present:

–The scatterers (particles or inhomogeneities) are statistically isotropic and no long-range order exists, *i.e.* there is no correlation between points at great spatial distance.

–The scatterers are embedded in a matrix. The matrix is considered to be a homogeneous medium with the electron density ρ_0. This situation holds for particles in solution or for inhomogeneities in a solid. The electron density in equations (2.6.1.3)–(2.6.1.5) should be replaced by the difference in electron density $\Delta\rho = \rho - \rho_0$, which can take positive and negative values.

The average over all orientations $\langle\ \rangle$ leads to

$$\langle\exp(-i\mathbf{h}\cdot\mathbf{r})\rangle = \frac{\sin hr}{hr} \qquad (2.6.1.6)$$

(Debye, 1915) and (2.6.1.4) reduces to the form

$$I(h) = 4\pi\int_0^\infty r^2\Delta\widetilde{\rho}^2(r)\frac{\sin hr}{hr}\ \mathrm{d}r \qquad (2.6.1.7)$$

or, with

$$p(r) = r^2\Delta\widetilde{\rho}^2(r) = r^2 V\gamma(r), \qquad (2.6.1.8)$$

to

$$I(h) = 4\pi\int_0^\infty p(r)\frac{\sin hr}{hr}\ \mathrm{d}r; \qquad (2.6.1.9)$$

γ is the so-called correlation function (Debye & Bueche, 1949), or characteristic function (Porod, 1951). The function $p(r)$ is the so-called pair-distance distribution function PDDF (Guinier &

Fournet, 1955; Glatter, 1979). The inverse transform to (2.6.1.9) is given by

$$p(r) = \frac{1}{2\pi^2} \int_0^\infty I(h) hr \sin(hr)\, \mathrm{d}h \qquad (2.6.1.10)$$

or by

$$V\gamma(r) = \frac{1}{2\pi^2} \int_0^\infty I(h) h^2 \frac{\sin hr}{hr}\, \mathrm{d}h. \qquad (2.6.1.11)$$

The function $p(r)$ is directly connected with the measurable scattering intensity and is very important for the solution of the inverse scattering problem. Before working out details, we should first discuss equations (2.6.1.9) and (2.6.1.10).

The PDDF can be defined as follows: the function $p(r)$ gives the number of difference electron pairs with a mutual distance between r and $r + \mathrm{d}r$ within the particle. For homogeneous particles (constant electron density), this function has a simple and clear geometrical definition.

Let us subdivide the particle into a very large number of identical small volume elements. The function $p(r)$ is proportional to the number of lines with a length between r and $r + \mathrm{d}r$ which are found in the combination of any volume element i with any other volume element k of the particle (see Fig. 2.6.1.1). For $r = 0$, there is no other volume element, so $p(r)$ must be zero, increasing with r^2 as the number of possible neighbouring volume elements is proportional to the surface of a sphere with radius r. Starting from an arbitrary point in the particle, there is a certain probability that the surface will be reached within the distance r. This will cause the $p(r)$ function to drop below the r^2 parabola and finally the PDDF will be zero for all $r > D$, where D is the maximum dimension of the particle. So $p(r)$ is a distance histogram of the particle. There is no information about the orientation of these lines in $p(r)$, because of the spatial averaging.

In the case of inhomogeneous particles, we have to weight each line by the product of the difference in electron density $\Delta\rho$, and the differential volume element, $\mathrm{d}V$. This can lead to negative contributions to the PDDF.

We can see from equation (2.6.1.9) that every distance r gives a $\sin(hr)/(hr)$ contribution with the weight $p(r)$ to the total scattering intensity. $I(h)$ and $p(r)$ contain the same information, but in most cases it is easier to analyse in terms of distances than in terms of $\sin(x)/x$ contributions. The PDDF could be computed exactly with equation (2.6.1.10) if $I(h)$ were known for the whole reciprocal space.

For $h = 0$, we obtain from equation (2.6.1.9)

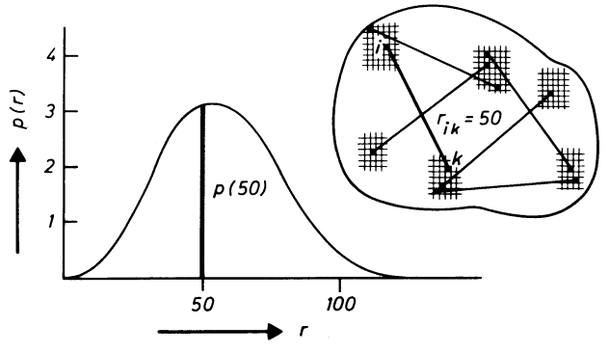

Fig. 2.6.1.1. The height of the $p(r)$ function for a certain value of r is proportional to the number of lines with a length between r and $r + \mathrm{d}r$ within the particle.

$$I(0) = I(\overline{\Delta\rho})^2 V^2 = 4\pi \int_0^\infty p(r)\, \mathrm{d}r, \qquad (2.6.1.12)$$

i.e. the scattering intensity at h equal to zero is proportional to the area under the PDDF. From equation (2.6.1.11), we find

$$V\gamma(0) = \frac{1}{2\pi^2} \int I(h) h^2\, \mathrm{d}h = V\overline{\Delta\rho^2} \qquad (2.6.1.13)$$

(Porod, 1982), *i.e.* the integral of the intensity times h^2 is related to the mean-square fluctuation of the electron density irrespective of the structure. We may modify the shape of a particle, the scattering function $I(h)$ might be altered considerably, but the integral (2.6.1.13) must remain invariant (Porod, 1951).

$$\text{Invariant } Q = \int_0^\infty I(h) h^2\, \mathrm{d}h. \qquad (2.6.1.14)$$

2.6.1.3. *Monodisperse systems*

In this subsection, we discuss scattering from monodisperse systems, *i.e.* all particles in the scattering volume have the same size, shape, and internal structure. These conditions are usually met by biological macromolecules in solution. Furthermore, we assume that these solutions are at infinite dilution, which is taken into account by measuring a series of scattering functions at different concentrations and by extrapolating these data to zero concentration. We continue with the notations defined in the previous subsection, which coincide to a large extent with the notations in the original papers and in the textbooks (Guinier & Fournet, 1955; Glatter & Kratky, 1982). There is a notation created by Luzzati (1960) that is quite different in many details. A comparison of the two notations is given in the Appendix of Pilz, Glatter & Kratky (1980).

The particles can be roughly described by some parameters that can be extracted from the scattering function. More information about the shape and structure of the particles can be found by detailed discussion of the scattering functions. At first, this discussion will be about homogeneous particles and will be followed by some aspects for inhomogeneous systems. Finally, we have to discuss the influence of finite concentrations on our results.

2.6.1.3.1. *Parameters of a particle*

Total scattering length. The scattering intensity at $h = 0$ must be equal to the square of the number of excess electrons, as follows from equations (2.6.1.7) and (2.6.1.12):

$$I(0) = (\Delta\rho)^2 V^2 = 4\pi \int_0^\infty p(r)\, \mathrm{d}r. \qquad (2.6.1.15)$$

This value is important for the determination of the molecular weight if we perform our experiments on an absolute scale (see below).

Radius of gyration. The electronic radius of gyration of the whole particle is defined in analogy to the radius of gyration in mechanics:

$$R_g^2 = \frac{\int_V \rho(r_i) r_i^2\, \mathrm{d}V_i}{\int_V \rho(r_i)\, \mathrm{d}V_i}. \qquad (2.6.1.16)$$

It can be obtained from the PDDF by

Table 2.6.1.1. *Formulae for the various parameters for h (left) and m (right) scales*

$R = K\sqrt{\tan\alpha}$ $\tan\alpha = \dfrac{\Delta \log I(h)}{\Delta h^2}$	$R = K\dfrac{\lambda a}{2\pi}\sqrt{\tan\alpha}$ $\tan\alpha = \dfrac{\Delta \log I(m)}{\Delta m^2}$
$K = \sqrt{\dfrac{3}{\log e}} = 2.628$	
$R_c = K_c\sqrt{\tan\alpha}$ $\tan\alpha = \dfrac{\Delta \log[I(h)h]}{\Delta h^2}$	$R_c = K_c\dfrac{\lambda a}{2\pi}\sqrt{\tan\alpha}$ $\tan\alpha = \dfrac{\Delta \log[I(m)m]}{\Delta m^2}$
$K_c = \sqrt{\dfrac{2}{\log e}} = 2.146$	
$R_t = K_t\sqrt{\tan\alpha}$ $\tan\alpha = \dfrac{\Delta \log[I(h)h^2]}{\Delta h^2}$	$R_t = K_t\dfrac{\lambda a}{2\pi}\sqrt{\tan\alpha}$ $\tan\alpha = \dfrac{\Delta \log[I(m)m^2]}{\Delta m^2}$
$K_t = \sqrt{\dfrac{1}{\log e}} = 1.517$	
$V = 2\pi^2\dfrac{I(0)}{Q}$ $Q = \int I(h)h^2\,\mathrm{d}h$	$V = \dfrac{\lambda^3 a^3}{4\pi}\dfrac{I(0)}{Q_m}$ $Q_m = \int I(m)m^2\,\mathrm{d}m$
$A = 2\pi\dfrac{[I(h)h]_0}{Q}$	$A = \dfrac{\lambda^2 a^2}{2\pi}\dfrac{[I(m)m]_0}{Q_m}$
$T = \pi\dfrac{[I(h)h^2]_0}{Q}$	$T = \dfrac{\lambda a}{2}\dfrac{[I(m)m^2]_0}{Q_m}$
$M = \dfrac{I(0)}{P}K\dfrac{a^2}{cd(\Delta z)^2}$	$K = \dfrac{1}{I_e N_L} = 21.0$
$M_c = \dfrac{[I(h)h]_0}{P}\dfrac{K}{\pi}\dfrac{a^2}{cd(\Delta z)^2}$	$M_c = \dfrac{[I(m)m]_0}{P}\dfrac{2K}{\lambda}\dfrac{a}{cd(\Delta z)^2}$
$M_t = \dfrac{[I(h)h^2]_0}{P}\dfrac{K}{2\pi}\dfrac{a^2}{cd(\Delta z)^2}$	$M_t = \dfrac{[I(m)m^2]_0}{P}\dfrac{2\pi K}{\lambda^2}\dfrac{1}{cd(\Delta z)^2}$
$\overline{(\Delta\rho)^2} = \dfrac{Q}{P}\dfrac{a^2}{2\pi^2 d}K$	$\overline{(\Delta\rho)^2} = \dfrac{Q_m}{P}\dfrac{4\pi}{\lambda^3 ad}K$
$K = 10^{24}/I_e$ $(10^{24} = [\mathrm{cm}/\text{Å}]^3)$	
$O_s = \pi\dfrac{K}{Q}$ $K = \lim\limits_{h\to\infty} I(h)h^4$	$O_s = \dfrac{2\pi^2}{\lambda a}\dfrac{K_m}{Q_m}$ $K = \lim\limits_{m\to\infty} I(m)m^4$

$$R_g^2 = \frac{\int_0^\infty p(r)r^2\,\mathrm{d}r}{2\int_0^\infty p(r)\,\mathrm{d}r} \qquad (2.6.1.17)$$

or from the innermost part of the scattering curve [Guinier approximation (Guinier, 1939)]:

$$I(h) = I(0)\exp(-h^2R_g^2/3). \qquad (2.6.1.18)$$

A plot of $\log[I(h)]$ *vs* h^2 (Guinier plot) shows at its innermost part a linear descent with a slope $\tan\alpha$, where

$$R_g = K\sqrt{\tan\alpha}$$

(see Table 2.6.1.1).

The radius of gyration is related to the geometrical parameters of simple homogeneous triaxial bodies as follows (Mittelbach, 1964):

sphere (radius R)	$R_g^2 = (3/5)R^2$
hollow sphere (radii R_1 and R_2)	$R_g^2 = (3/5)\dfrac{R_2^5 - R_1^5}{R_2^3 - R_1^3}$
ellipsoid (semi-axes a, b, c)	$R_g^2 = (1/5)(a^2 + b^2 + c^2)$
parallelepiped (edge lengths A, B, C)	$R_g^2 = (1/12)(A^2 + B^2 + C^2)$
elliptic cylinder (semi-axes a, b; height h)	$R_g^2 = \dfrac{a^2 + b^2}{4} + \dfrac{h^2}{12} = R_c^2 + \dfrac{h^2}{12}$
hollow cylinder (height h and radii r_1, r_2)	$R_g^2 = \dfrac{r_1^2 + r_2^2}{2} + \dfrac{h^2}{12}$.

Radius of gyration of the cross section. In the special case of rod-like particles, the two-dimensional analogue of R_g is called radius of gyration of the cross section R_c. It can be obtained from

$$R_c^2 = \frac{\int_0^\infty p_c(r)r^2\,\mathrm{d}r}{2\int_0^\infty p_c(r)\,\mathrm{d}r}, \qquad (2.6.1.19)$$

where $p_c(r)$ is the PDDF of the cross section or it can be calculated from the innermost part of the scattering intensity of the cross section $I_c(h)$:

$$I_c(h) = I_c(0)\exp(-h^2R_c^2/2), \qquad (2.6.1.20)$$

with $I_c(h) = I(h)h$ (see Table 2.6.1.1).

Radius of gyration of the thickness. A similar definition exists for lamellar particles. The one-dimensional radius of gyration of the thickness R_t can be calculated from

$$R_t^2 = \frac{\int_0^\infty p_t(r)r^2\,\mathrm{d}r}{2\int_0^\infty p_t(r)\,\mathrm{d}r}, \qquad (2.6.1.21)$$

or from the innermost part of the scattered intensity of thickness $I_t(h)$:

$$I_t(h) = I_t(0)\exp(-h^2R_t^2), \qquad (2.6.1.22)$$

with $I_t(h) = I(h)h^2$ (see Table 2.6.1.1 and §2.6.1.3.2.1).

Volume. The volume of a homogeneous particle is given by

$$V = 2\pi^2\frac{I(0)}{Q}. \qquad (2.6.1.23)$$

This equation follows from equations (2.6.1.12)–(2.6.1.14). Such volume determinations are subject to errors as they rely on the validity of an extrapolation to zero angle [to obtain $I(0)$] and to larger angles (h^{-4} extrapolation for Q). Scattering functions cannot be measured from h equal to zero to h equal to infinity.

Surface. The surface S of one particle is correlated with the scattering intensity $I_1(h)$ of this particle by

$$I_1(h)|_{h\to\infty} = (\Delta\rho)^2 \frac{2\pi}{h^4} S. \qquad (2.6.1.24)$$

Determination of the absolute intensity can be avoided if we calculate the specific surface O_s (Mittelbach & Porod, 1965)

$$O_s = S/V = \pi \frac{\lim_{h\to\infty} [I(h)h^4]}{Q}. \qquad (2.6.1.25)$$

Cross section, thickness, and correlation length. By similar equations, we can find the area A of the cross section of a rod-like particle

$$A = 2\pi \frac{[I(h)h]_{h\to 0}}{Q} \qquad (2.6.1.26)$$

and the thickness T of lamellar particles by

$$T = \pi \frac{[I(h)h^2]_{h\to 0}}{Q} \qquad (2.6.1.27)$$

but the experimental accuracy of the limiting values $[I(h)h]_{h\to 0}$ and $[I(h)h^2]_{h\to 0}$ is usually not very high.

The correlation length l_c is the mean width of the correlation function $\gamma(r)$ (Porod, 1982) and is given by

$$l_c = \frac{\pi}{Q} \int_0^\infty I(h)h \, \mathrm{d}h. \qquad (2.6.1.28)$$

The *maximum dimension* D of a particle would be another important particle parameter, but it cannot be calculated directly from the scattering function and will be discussed later.

Persistence length a_p. An important model for polymers in solution is the so-called worm-like chain (Porod, 1949; Kratky & Porod, 1949). The degree of coiling can be characterized by the persistence length a_p (Kratky, 1982*b*). Under the assumption that the persistence length is much larger than the cross section of the polymer, it is possible to find a transition point h^+ in an $I(h)h^2$ *vs* h plot where the function starts to be proportional to h. There is an approximation

$$h^+ a_p \simeq 2.3, \qquad (2.6.1.29)$$

depending on the length of the chain (Heine, Kratky & Roppert, 1962). For further details, see Kratky (1982*b*).

Molecular weight. Particles of arbitrary shape. The particle is measured at high dilution in a homogeneous solution and has an isopotential specific volume v_2' and z_2 mol. electrons per gram, *i.e.* the molecule contains $z_2 M$ electrons if M is the molecular weight. The number of effective mol. electrons per gram is given by

$$\Delta z_2 = (z_2 - v_2'\rho_0), \qquad (2.6.1.30)$$

where ρ_0 is the mean electron density of the solvent. The molecular weight can be determined from the intensity at zero angle $I(0)$:

$$M = \frac{I(0)}{P} \frac{a^2}{\Delta z^2 dc I_e N_L} = \frac{I(0)}{P} \frac{21.0a^2}{\Delta z^2 dc} \qquad (2.6.1.31)$$

(Kratky, Porod & Kahovec, 1951), where P is the total intensity per unit time irradiating the sample, a [cm] is the distance between the sample and the plane of registration, d [cm] is the thickness of the sample, c [g cm^{-3}] is the concentration, and N_L is Loschmidt's (Avogadro's) number.

Rod-like particles. The mass per unit length $M_c = M/L$, *i.e.* the mass related to the cross section of a rod-like particle with length L, is given by a similar equation (Kratky & Porod, 1953):

$$M_c = \frac{[I(h)h]_{h\to 0}}{P} \frac{a^2}{\pi \Delta z^2 dc I_e N_L} = \frac{[I(h)h]_{h\to 0}}{P} \frac{6.68a^2}{\Delta z^2 dc}. \qquad (2.6.1.32)$$

Flat particles. A similar equation holds for the mass per unit area $M_t = M/A$:

$$M_t = \frac{[I(h)h^2]_{h\to 0}}{P} \frac{a^2}{2\pi \Delta z^2 dc I_e N_L} = \frac{[I(h)h^2]_{h\to 0}}{P} \frac{3.34a^2}{\Delta z^2 dc}. \qquad (2.6.1.33)$$

Abscissa scaling. The various molecular parameters can be evaluated from scattered intensities with different abscissa scaling. The abscissa used in theoretical work is $h = (4\pi/\lambda)\sin\theta$. The most important experimental scale is m [cm], the distance of the detector from the centre of the primary beam with the distance a [cm] between the sample and the detector plane.

$$h[\mathrm{nm}^{-1}] = T_{hm}[\mathrm{cm}^{-1}\mathrm{nm}^{-1}]m[\mathrm{cm}], \qquad (2.6.1.34)$$

with

$$T_{hm} = 2\pi/\lambda a. \qquad (2.6.1.35)$$

The angular scale 2θ with

$$2\theta \simeq m/a = (\lambda/2\pi)h \qquad (2.6.1.36)$$

was used in the early years of small-angle X-ray scattering experiments. The formulae for the various parameters for m and the h scale can be found in Table 2.6.1.1, the formulae for the 2θ scale can be found in Glatter & Kratky (1982, p. 158).

2.6.1.3.2. *Shape and structure of particles*

In this subsection, we have to discuss how shape, size, and structure of the scattering particle are reflected in the scattering function $I(h)$ and in the PDDF $p(r)$. In general, it is easier to discuss features of the PDDF, but some characteristics like symmetry give more pronounced effects in reciprocal space.

2.6.1.3.2.1. *Homogeneous particles*

Globular particles. Only a few scattering problems can be solved analytically. The most trivial shape is a sphere. Here we have analytical expressions for the scattering intensity

$$I(h) = \left(3\frac{\sin(hR) - hR\cos(hR)}{(hR)^3}\right)^2 \qquad (2.6.1.37)$$

and for the PDDF (Porod, 1948)

$$p(r) = 12x^2(2 - 3x + x^3) \quad x = r/(2R) \le 1, \qquad (2.6.1.38)$$

where R is the radius of the sphere. The graphical representation of scattering functions is usually made with a semi-log plot [$\log I(h)$ *vs* h] or with a log–log plot [$\log I(h)$ *vs* $\log h$]; the PDDF is shown in a linear plot. In order to compare functions from particles of different shape, it is preferable to keep the scattering intensity at zero angle (area under PDDF) and the radius of

gyration R_g [slope of the main maximum of $I(h)$ or the second moment of $p(r)$] constant.

The scattering function of a sphere with $R = 65$ is shown in Fig. 2.6.1.2 [dashed line, $\log I(0)$ normalized to 12]. We see distinct minima which are typical for particles of high symmetry. We can determine the size of the sphere directly from the position of the zeros h_{01} and h_{02} (Glatter, 1972).

$$R \simeq \frac{4.493}{h_{01}} \quad \text{or} \quad R \simeq \frac{7.725}{h_{02}} \tag{2.6.1.39}$$

or from the position of the first side maximum ($R_g \simeq 4.5/h_1$). The minima are considerably flattened in the case of cubes (full line in Fig. 2.6.1.2). The corresponding differences in real space are not so clear-cut (Fig. 2.6.1.3). The $p(r)$ function of the sphere has a maximum near $r = R = D/2$ ($x \simeq 0.525$) and drops to zero like every PDDF at $r = D$, where D is the maximum dimension of the particle – here the diameter. The $p(r)$ for the cube with the same R_g is zero at $r \simeq 175$. The function is very flat in this region. This fact demonstrates the problems of accuracy in this determination of D when we take into account experimental errors. In any case, this accuracy will be different for different shapes.

Any deviation from spherical symmetry will shift the maximum to smaller r values and the value for D will increase [$I(0)$ and R_g constant!]. A comparison of PDDF's for a sphere, an oblate ellipsoid of revolution (axial ratio 1:1:0.2), and a prolate ellipsoid of revolution (1:1:3) is shown in Fig. 2.6.1.4. The more we change from the compact, spherical structure to a two- and one-dimensionally elongated structure, the more the maximum shifts to smaller r values and at the same time we have an increase in D. We see that $p(r)$ is a very informative function. The interpretation of scattering functions in reciprocal space is hampered by the highly abstract nature of this domain. We can see this problem in Fig. 2.6.1.5, where the scattering functions of the sphere and the ellipsoids in Fig. 2.6.1.4 are plotted. A systematic discussion of the features of $p(r)$ can be found elsewhere (Glatter, 1979, 1982*b*).

Rod-like particles. The first example of a particle elongated in one direction (prolate ellipsoid) was given in Figs. 2.6.1.4 and 2.6.1.5. An important class is particles elongated in one

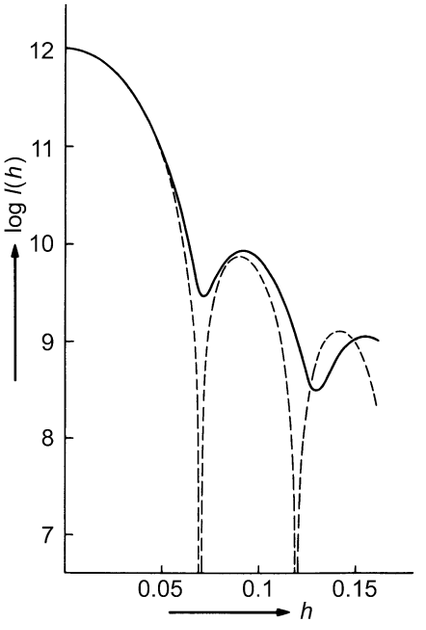

Fig. 2.6.1.2. Comparison of the scattering functions of a sphere (- - - -) and a cube (———) with same radius of gyration.

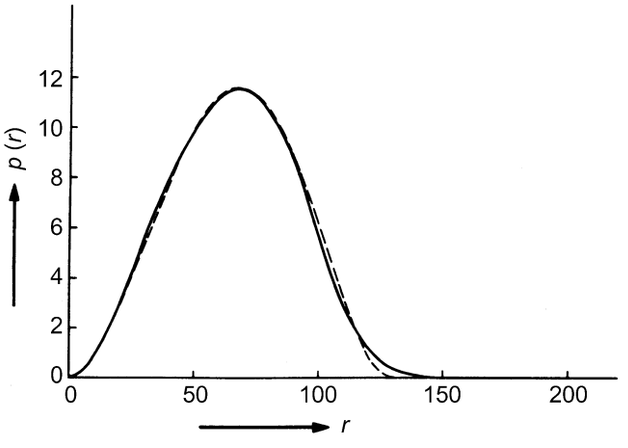

Fig. 2.6.1.3. Distance distribution function of a sphere (- - - -) and a cube (———) with the same radius of gyration and the same scattering intensity at zero angle.

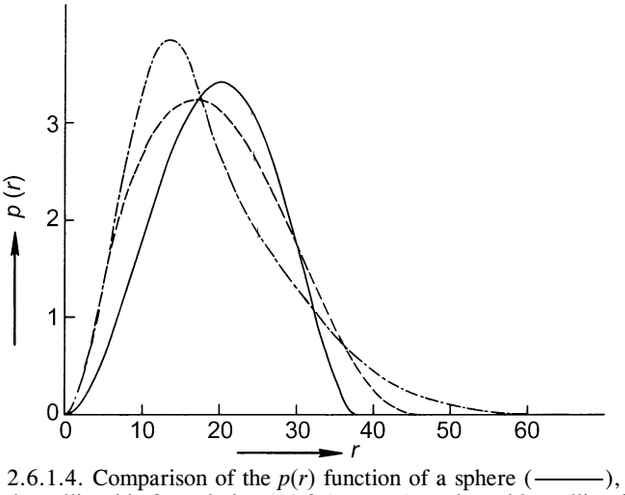

Fig. 2.6.1.4. Comparison of the $p(r)$ function of a sphere (———), a prolate ellipsoid of revolution 1:1:3 (—·—·—), and an oblate ellipsoid of revolution 1:1:0.2 (- - - -) with the same radius of gyration.

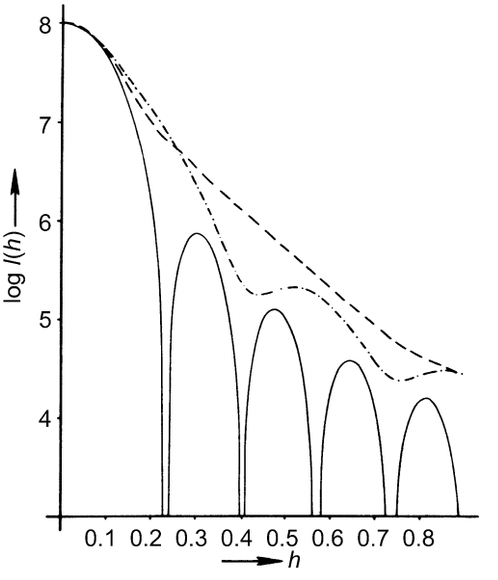

Fig. 2.6.1.5. Comparison of the $I(h)$ functions of a sphere, a prolate, and an oblate ellipsoid (see legend to Fig. 2.6.1.4).

direction with a constant cross section of arbitrary shape (long cylinders, parallelepipeds, *etc.*) The cross section A (with maximum dimension d) should be small in comparison to the length of the whole particle L:

$$d \ll L \quad L = (D^2 - d^2)^{1/2} \simeq D. \tag{2.6.1.40}$$

The scattering curve of such a particle can be written as

$$I(h) = L(\pi/h)I_c(h), \tag{2.6.1.41}$$

where the function $I_c(h)$ is related only to the cross section and the factor $1/h$ is characteristic for rod-like particles (Kratky & Porod, 1948; Porod, 1982). The cross-section function $I_c(h)$ is

$$I_c(h) = (L\pi)^{-1}I(h)h = \text{constant} \times I(h)h. \tag{2.6.1.42}$$

This function was used in the previous subsection for the determination of the cross-section parameters R_c, A, and M_c. In addition, we have

$$I_c(h) = 2\pi \int_0^\infty p_c(r)J_0(hr)\,\mathrm{d}r, \tag{2.6.1.43}$$

where $J_0(hr)$ is the zero-order Bessel function and

$$p_c(r) = \frac{1}{2\pi}\int_0^\infty I_c(h)(hr)J_0(hr)\,\mathrm{d}h \tag{2.6.1.44}$$

(Glatter, 1982*a*). The function $p_c(r)$ is the PDDF of the cross section with

$$p_c(r) = r\gamma_c(r) = \langle \Delta\rho(\mathbf{r}_c) * \Delta\rho(-\mathbf{r}_c)\rangle. \tag{2.6.1.45}$$

The symbol * stands for the mathematical operation called convolution and the symbol $\langle\ \rangle$ means averaging over all directions in the plane of the cross section. Rod-like particles with a constant cross section show a linear descent of $p(r)$ for $r \gg d$ if $D > 2.5d$. The slope of this linear part is proportional to the square of the area of the cross section,

$$\frac{\mathrm{d}p}{\mathrm{d}r} = -\frac{A^2\Delta\rho^2}{2}. \tag{2.6.1.46}$$

The PDDF's of parallelepipeds with the same cross section but different length L are shown in Fig. 2.6.1.6. The maximum corresponds to the cross section and the point of inflection r_i gives a rough indication for the size of the cross section. This is shown more clearly in Fig. 2.6.1.7, where three parallelepipeds with equal cross section area A but different cross-section dimensions are shown. If we find from the overall PDDF that the particle under investigation is a rod-like particle, we can use the PDDF of the cross section $p_c(r)$ to obtain more information on the cross section (Glatter, 1980*a*).

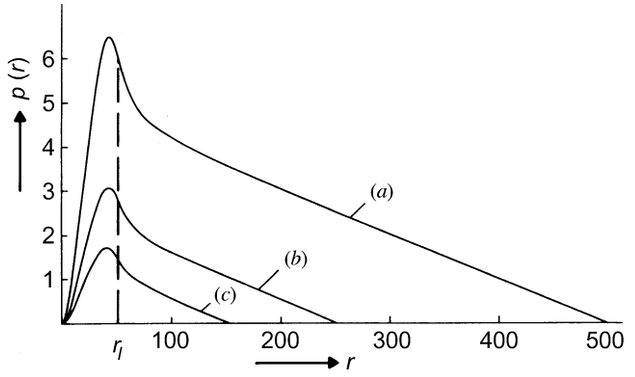

Fig. 2.6.1.6. Distance distributions from homogeneous parallelepipeds with edge lengths of: (*a*) 50 × 50 × 500 Å; (*b*) 50 × 50 × 250 Å; (*c*) 50 × 50 × 150 Å.

Flat particles. Flat particles, *i.e.* particles elongated in two dimensions (discs, flat parallelepipeds), with a constant thickness T much smaller than the overall dimensions D, can be treated in a similar way. The scattering function can be written as

$$I(h) = A\frac{2\pi}{h^2}I_t(h), \tag{2.6.1.47}$$

where $I_t(h)$ is the so-called thickness factor (Kratky & Porod, 1948) or

$$I_t(h) = (A2\pi)^{-1}I(h)h = \text{constant} \times I(h)h^2, \tag{2.6.1.48}$$

which can be used for the determination of R_t, T, and M_t. In addition, we have again:

$$I_t(h) = 2\int_0^\infty p_t(r)\cos(hr)\,\mathrm{d}r \tag{2.6.1.49}$$

and

$$p_t(r) = \gamma_t(r) - \frac{1}{\pi}\int_0^\infty I_t(h)\cos(hr)\,\mathrm{d}h$$
$$= \Delta\rho_t(r) * \Delta\rho_t(-r). \tag{2.6.1.50}$$

PDDF's from flat particles do not show clear features and therefore it is better to study $f(r) = p(r)/r$ (Glatter, 1979). The corresponding functions for lamellar particles with the same basal plane but different thickness are shown in Fig. 2.6.1.7(*b*). The marked transition points in Fig. 2.6.1.7(*b*) can be used to determine the thickness. The PDDF of the thickness $p_t(r)$ can give more information in such cases, especially for inhomogeneous particles (see below).

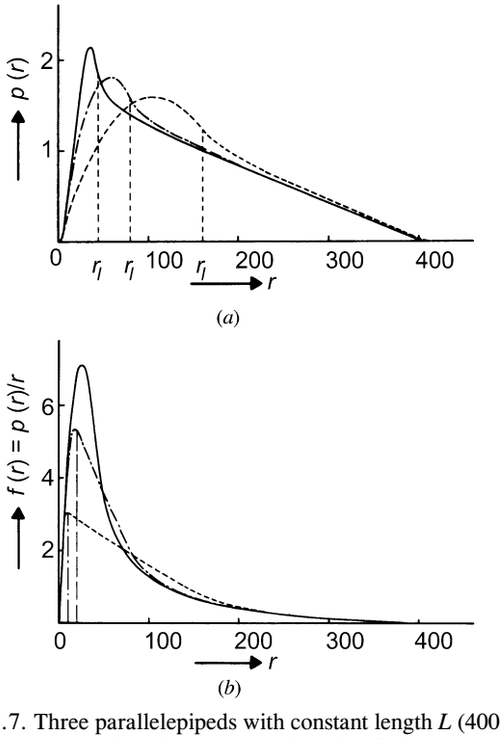

Fig. 2.6.1.7. Three parallelepipeds with constant length L (400 Å) and a constant cross section but varying length of the edges: ——— 40 × 40 Å; —·—·— 80 × 20 Å; - - - - 160 × 10 Å. (*a*) $p(r)$ function. (*b*) $f(r) = p(r)/r$.

Composite structures – aggregates, subunits. The formation of dimers can be analysed qualitatively with the $p(r)$ function (Glatter, 1979). For an approximate analysis, it is only necessary to know the PDDF of the monomer. Different types of aggregates will have distinct differences in their PDDF. Higher aggregates generally cannot be classified unambiguously. Additional information from other sources, such as the occurrence of symmetry, can simplify the problem.

Particles that consist of aggregates of a relatively large number of identical subunits show, at low resolution, the overall structure of the whole particle. At larger angles (higher resolution), the influence of the individual subunits can be seen. In the special case of globular subunits, it is possible to determine the size of the subunits from the position of the minima of the corresponding shape factors using equation (2.6.1.39) (Glatter, 1972; Pilz, Glatter, Kratky & Moring-Claesson, 1972).

2.6.1.3.2.2. *Hollow and inhomogeneous particles*

We have learned to classify homogeneous particles in the previous part of this section. It is possible to see from scattering data [$I(h)$ or $p(r)$] whether a particle is globular or elongated, flat or rod-like, *etc*., but it is impossible to determine uniquely a complicated shape with many parameters. If we allow internal inhomogeneities, we make things more complicated and it is clear that it is impossible to obtain a unique reconstruction of an inhomogeneous three-dimensional structure from its scattering function without additional *a priori* information. We restrict our considerations to special cases that are important in practical applications and that allow at least a solution in terms of a first-order approximation. In addition, we have to remember that the $p(r)$ function is weighted by the number of excess electrons that can be negative. Therefore, a minimum in the PDDF can be caused by a small number of distances, or by the addition of positive and negative contributions.

Spherically symmetric particles. In this case, it is possible to describe the particle by a one-dimensional radial excess density function $\Delta\rho(r)$. For convenience, we omit the Δ sign for excess in the following. As we do not have any angle-dependent terms, we have no loss of information from the averaging over angle. The scattering amplitude is simply the Fourier transform of the radial distribution:

$$A(h) = 4\pi \int_0^\infty r\rho(r)\frac{\sin(hr)}{h}\,\mathrm{d}r \qquad (2.6.1.51)$$

$[I(h) - A(h)^2]$ and

$$\rho(r) = \frac{1}{2\pi^2}\int_0^\infty hA(h)\frac{\sin(hr)}{r}\,\mathrm{d}h \qquad (2.6.1.52)$$

(Glatter, 1977*a*). These equations would allow direct analysis if $A(h)$ could be measured, but we can measure only $I(h)$. $\rho(r)$ can be calculated from $I(h)$ using equation (2.6.1.10) remembering that this function is the convolution square of $\rho(r)$ [equations (2.6.1.5) and (2.6.1.8)]. Using a *convolution square-root* technique, we can calculate $\rho(r)$ from $I(h)$ *via* the PDDF without having a 'phase problem' like that in crystallography; *i.e*. it is not necessary to calculate scattering amplitudes and phases (Glatter, 1981; Glatter & Hainisch, 1984; Glatter, 1988). This can be done because $p(r)$ differs from zero only in the limited range $0 < r < D$ (Hosemann & Bagchi, 1952, 1962). In mathematical terms, it is again the difference between a Fourier series and a Fourier integral.

Details of the technique cannot be discussed here, but it is a fact that we can calculate the radial distribution $\rho(r)$ from the scattering data assuming that the spherical scatterer is only of finite size. The hollow sphere can be treated either as a homogeneous particle with a special shape or as an inhomogeneous particle with spherical symmetry with a step function as radial distribution. The scattering function and the PDDF of a hollow sphere can be calculated analytically. The $p(r)$ of a hollow sphere has a triangular shape and the function $f(r) = p(r)/r$ shows a horizontal plateau (Glatter, 1982*b*).

Rod-like particles. Radial inhomogeneity. If we assume radial inhomogeneity of a circular cylinder, *i.e*. ρ is a function of the radius r but not of the angle φ or of the value of z in cylindrical coordinates, we can determine some structural details. We define $\bar{\rho}_c$ as the average excess electron density in the cross section. Then we obtain a PDDF with a linear part for $r > d$ and we have to replace $\Delta\rho$ in equation (2.6.1.46) by $\bar{\rho}_c$ with the maximum dimension of the cross section d. The $p(r)$ function differs from that of a homogeneous cylinder with the same $\bar{\rho}_c$ only in the range $0 < r \leq d$. A typical example is shown in Fig. 2.6.1.8. The functions for a homogeneous, a hollow, and an inhomogeneous cylinder with varying density $\rho_c(r)$ are shown.

Rod-like particles. Axial inhomogeneity. This is another special case for rod-like particles, *i.e*. the density is a function of the z coordinate. In Fig. 2.6.1.9, we compare two cylinders with the same size and diameter. One is a homogeneous cylinder with density $\bar{\rho}$, diameter $d = 48$ and length $L = 480$, and the other is an inhomogeneous cylinder of the same size and mean density $\bar{\rho}$, but this cylinder is made from slices with a thickness of 20 and alternating densities of $1.5\bar{\rho}$ and $0.5\bar{\rho}$, respectively. The PDDF of the inhomogeneous cylinder has ripples with the periodicity of 40 in the whole linear range. This periodicity leads to reflections in reciprocal space (first and third order in the h range of the figure).

Flat particles. Cross-sectional inhomogeneity. Lamellar particles with varying electron density perpendicular to the basal plane, where ρ is a function of the distance x from the central plane, show differences from a homogeneous lamella of the same size in the PDDF in the range $0 < r < T$, where T is the

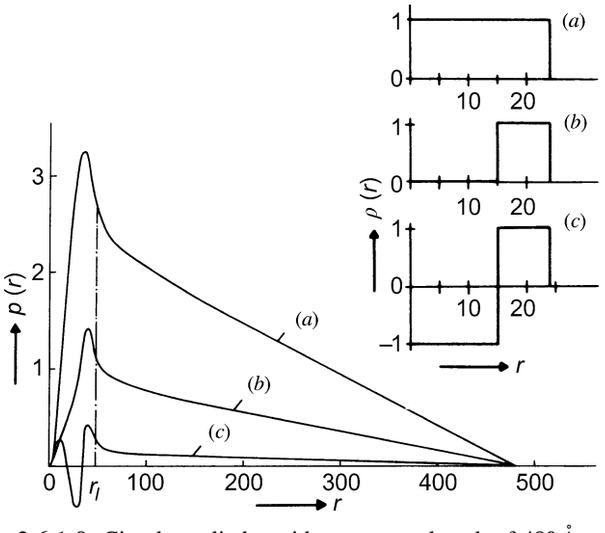

Fig. 2.6.1.8. Circular cylinder with a constant length of 480 Å and an outer diameter of 48 Å. (*a*) Homogeneous cylinder, (*b*) hollow cylinder, (*c*) inhomogeneous cylinder. The $p(r)$ functions are shown on the left, the corresponding electron-density distributions $\rho(r)$ on the right.

thickness of the lamella. An example is given in Fig. 2.6.1.10 where we compare a homogeneous lamellar particle (with $\rho = +\frac{1}{3}$) with an inhomogeneous one, $\rho_t(x)$ being a three-step function alternating between the values $+1$, -1, $+1$.

Flat particles. In-plane inhomogeneity. Lamellae with a homogeneous cross section but inhomogeneities along the basal plane have a PDDF that deviates from that of a homogeneous lamella in the whole range $0 < r < D$. These deviations are a measure of the in-plane inhomogeneites; a general evaluation method does not exist. Even more complicated is the situation that occurs in membranes: these have a pronounced cross-sectional structure with additional in-plane inhomogeneities caused by the membrane proteins (Laggner, 1982; Sadler & Worcester, 1982).

Contrast variation and labelling. An important method for studying inhomogeneous particles is the method of contrast variation (Stuhrmann, 1982). By changing the contrast of the solvent, we can obtain additional information about the inhomogeneities in the particles. This variation of the contrast is much easier for neutron scattering than for X-ray scattering because hydrogen and deuterium have significantly different scattering cross sections. This technique will therefore be discussed in the section on neutron small-angle scattering.

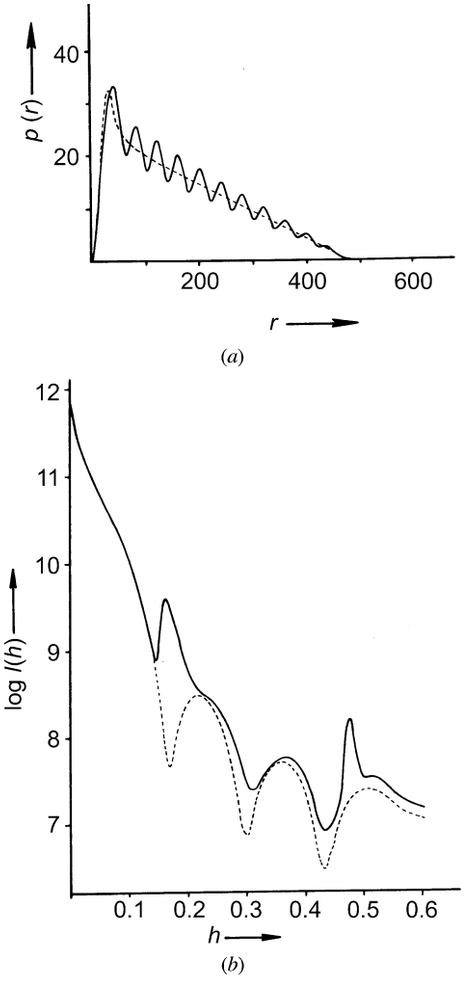

Fig. 2.6.1.9. Inhomogeneous circular cylinder with periodical changes of the electron density along the cylinder axis compared with a homogeneous cylinder with the same mean electron density. (*a*) $p(r)$ function; (*b*) scattering intensity; ——— inhomogeneous cylinder; - - - - homogeneous cylinder.

A method for distance determination with X-rays by heavy-atom labelling was developed by Kratky & Worthman (1947). These ideas are now used for the determination of distances between deuterated subunits of complex macromolecular structures with neutron scattering.

High-resolution experiments. A special type of study is the comparison of the structures of the same molecule in the crystal and in solution. This is done to investigate the influence of the crystal field on the polymer structure (Krigbaum & Kügler, 1970; Damaschun, Damaschun, Müller, Ruckpaul & Zinke, 1974; Heidorn & Trewhella, 1988) or to investigate structural changes (Ruckpaul, Damaschun, Damaschun, Dimitrov, Jänig, Müller, Pürschel & Behlke, 1973; Hubbard, Hodgson & Doniach, 1988). Sometimes such investigations are used to verify biopolymer structures predicted by methods of theoretical physics (Müller, Damaschun, Damaschun, Misselwitz, Zirwer & Nothnagel, 1984). In all cases, it is necessary to measure the small-angle scattering curves up to relatively high scattering angles ($h \simeq 30\,\mathrm{nm}^{-1}$, and more). Techniques for such experiments have been developed during recent years (Damaschun, Gernat, Damaschun, Bychkova & Ptitsyn, 1986; Gernat, Damaschun, Kröber, Bychkova & Ptitsyn, 1986; I'anson, Bacon, Lambert, Miles, Morris, Wright & Nave, 1987) and need special evaluation methods (Müller, Damaschun & Schrauber, 1990).

2.6.1.3.3. *Interparticle interference, concentration effects*

So far, only the scattering of single particles has been treated, though, of course, a great number of these are always present. It has been assumed that the intensities simply add to give the total diffraction pattern. This is true for a very dilute solution, but with increasing concentration interference effects will contribute. Biological samples often require higher concentrations for a sufficient signal strength. We can treat this problem in two different ways:

–We accept the interference terms as additional information about our system under investigation, thus observing the spatial arrangement of the particles.

–We treat the interference effect as a perturbation of our single-particle concept and discuss how to remove it.

The first point of view is the more general, but there are many open questions left. For many practical applications, the second point of view is important.

The radial distribution function. In order to find a general description, we have to restrict ourselves to an isotropic assembly of monodisperse spheres. This makes it possible to

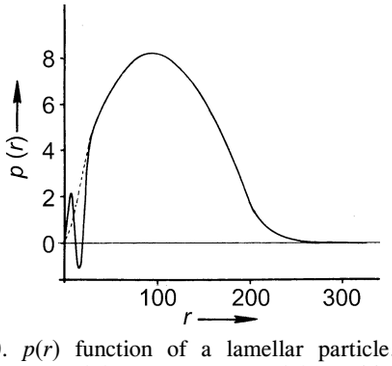

Fig. 2.6.1.10. $p(r)$ function of a lamellar particle. The full line corresponds to an inhomogeneous particle, $\rho_t(x)$ is a three-step function with the values $+1$, -1, $+1$. The broken line represents the homogeneous lamella with $\rho = +\frac{1}{3}$.

describe the situation by introducing a radial interparticle distribution function $P(r)$ (Zernicke & Prins, 1927; Debye & Menke, 1930). Each particle has the same surroundings. We consider one central particle and ask for the probability that another particle will be found in the volume element $\mathrm{d}V$ at a distance r apart. The mean value is $(N/v)\,\mathrm{d}V$; any deviation from this may be accounted for by a factor $P(r)$. In the range of impenetrability ($r < D$), we have $P(r) = 0$ and in the long range ($r \gg D$) $P(r) = 1$. So the corresponding equation takes the form

$$I(h) = NI_1(h)\left[1 + \frac{N}{V}\int_0^\infty 4\pi r^2[P(r) - 1]\frac{\sin(hr)}{hr}\,\mathrm{d}r\right]. \quad (2.6.1.53)$$

The second term contains all interparticle interferences. Its predominant part is the 'hole' of radius D, where $[P(r) - 1] = -1$. This leads to a decrease of the scattering intensity mainly in the central part, which results in a liquid-type pattern (Fig. 2.6.1.11). This can be explained by the reduction of the contrast caused by the high number of surrounding particles. Even if a size distribution for the spheres is assumed, the effect remains essentially the same (Porod, 1952). Up to now, no exact analytical expressions for $P(r)$ exist. The situation is even more complicated if one takes into account attractive or repulsive interactions or non-spherical particle shapes (orientation).

If we have a system of spheres with known size D, we can use equation (2.6.1.37) for $I_1(h)$ in equation (2.6.1.53), divide by this function, and calculate $P(r)$ from experimental data by Fourier inversion. The interference term can be used to study particle correlations of charged macromolecular solutions (Chen, Sheu, Kalus & Hoffmann, 1988).

If there are attractive forces, there will be a tendency for aggregation. This tendency may, for instance, be introduced by some steps in the procedure of preparation of biological samples. Such aggregation leads to an increase of the intensity in the central part (gas type). In this case, we will finally have a polydisperse system of monomers and oligomers. Again, there exist no methods to analyse such a system uniquely.

Elimination of concentration effects – liquid type. In most cases, the interference effect is a perturbation of our experiment where we are only interested in the particle scattering function. Any remaining concentration effect would lead to errors in the resulting parameters. As we have seen above, the effect is essential at low h values, thus influencing $I(0)$, R_g, and the PDDF at large r values.

The problem can be handled for the liquid-like type in the following way. We measure the scattering function $I(h)$ at different concentrations (typically from a few $\mathrm{mg\,ml^{-1}}$ up to about $50\,\mathrm{mg\,ml^{-1}}$). The influence of the concentration can be seen in a common plot of these scattering curves, divided by their concentrations. For large h values, these curves are identical. In the low-h range, the curves must be extrapolated to zero concentration. It depends on the problem as to whether a linear fit is sufficient or whether a second-degree polynomial has to be used. The extrapolation can be performed in a standard $I(h)/c$ *versus* h plot or in a Zimm plot $[I(h)/c]^{-1}$ *versus* h (Cleemann & Kratky, 1960; Kirste & Oberthür, 1982). The Zimm plot should be preferred when working with highly concentrated solutions (Pilz, 1982).

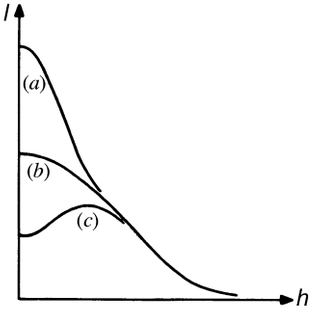

Fig. 2.6.1.11. Characteristic types of scattering functions: (*a*) gas type; (*b*) particle scattering; (*c*) liquid type.

As mentioned above, the innermost part of the scattering function is lowered and the apparent radius of gyration decreases with increasing concentration. The length of the linear range of the Guinier plot can be extended by the interference effect for non-spherical particles. Thus, an elongated linear Guinier plot is no guarantee of the completeness of the elimination of the concentration effect. Remaining interparticle interferences cannot be recognized in reciprocal space.

The PDDF is affected considerably by interparticle interference (Glatter, 1979). It is lowered with increasing distance r, goes through a negative minimum in the region of the maximum dimension D of the particle, and the oscillations vanish at larger r values. This is shown for the hard-sphere model in Fig. 2.6.1.12. The oscillations disappear when the concentration goes to zero.

The same behaviour can be found from experimental data even in the case of non-spherical data (Pilz, Goral, Hoylaerts, Witters & Lontie, 1980; Pilz, 1982).

In some cases, it may be impossible to carry out experiments with varying concentrations. This will be the case if the structure of the particles depends on concentration. Under certain circumstances, it is possible to find the particle parameters by neglecting the innermost part of the scattering function influenced by the concentration effect (Müller & Glatter, 1982).

Aggregates – gas type. When the particles show a tendency to aggregation with increasing concentration, we can follow the same procedures as discussed for the liquid type, *i.e.* perform a concentration series and extrapolate the $I(h)/c$ curves to zero concentration.

However, in most cases, the tendency to aggregation exists at any concentration, *i.e.* even at very high dilution we have a certain number of oligomers coexisting with monomers. There is no unique way to find the real particle parameters in these cases. It is not sufficient just to neglect the innermost part of the

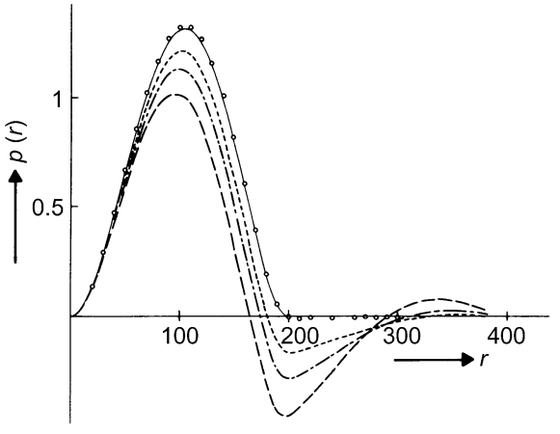

Fig. 2.6.1.12. Distance distribution – hard-sphere interference model. Theoretical $p(r)$ functions: ——— $\theta = 0$; - - - $\theta = 0.25$; —·—·— $\theta = 0.5$; — — — $\theta = 1.0$. Circles: results from indirect transformation: $\theta = 0.5$, $h_1R = 2.0$. 2% statistical noise, $D_{\max} = 300\,\text{Å}$, $\Delta R_g = 0.5\%$, $\Delta I_0 = 1.2\%$.

scattering function because that leads to an increasing loss of essential information about the particle (monomer) itself.

2.6.1.4. *Polydisperse systems*

In this subsection, we give a short survey of the problem of polydispersity. It is most important that there is no way to decide from small-angle scattering data whether the sample is mono- or polydisperse. Every data set can be evaluated in terms of monodisperse or polydisperse structures. Independent *a priori* information is necessary to make this decision. It has been shown analytically that a certain size distribution of spheres gives the same scattering function as a monodisperse ellipsoid with axes a, b and c (Mittelbach & Porod, 1962).

The scattering function of a polydisperse system is determined by the shape of the particles and by the size distribution. As mentioned above, we can assume a certain size distribution and can determine the shape, or, more frequently, we assume the shape and determine the size distribution. In order to do this we have to assume that the scattered intensity results from an ensemble of particles of the same shape whose size distribution can be described by $D_n(R)$, where R is a size parameter and $D_n(R)$ denotes the number of particles of size R. Let us further assume that there are no interparticle interferences or multiple scattering effects. Then the scattering function $I(h)$ is given by

$$I(h) = c_n \int_0^\infty D_n(R) R^6 i_0(hR)\, \mathrm{d}R, \qquad (2.6.1.54)$$

where c_n is a constant, the factor R^6 takes into account the fact that the particle volume is proportional to R^3, and $i_0(hR)$ is the normalized form factor of a particle size R. In many cases, one is interested in the mass distribution $D_m(R)$ [sometimes called volume distribution $D_c(R)$]. In this case, we have

$$I(h) = c_m \int_0^\infty D_m(R) R^3 i_0(hR)\, \mathrm{d}R. \qquad (2.6.1.55)$$

The solution of these integral equations, *i.e.* the computation of $D_n(R)$ or $D_m(R)$ from $I(h)$, needs rather sophisticated numerical or analytical methods and will be discussed later.

The problems of interparticle interference and multiple scattering in the case of polydisperse systems cannot be described analytically and have not been investigated in detail up to now. In general, interference effects start to influence data from small-angle scattering experiments much earlier, *i.e.* at lower concentration, than multiple scattering. Multiple scattering becomes more important with increasing size and contrast and is therefore dominant in light-scattering experiments in higher concentrations.

A concentration series and extrapolation to zero concentration as in monodisperse systems should be performed to eliminate these effects.

2.6.1.5. *Instrumentation*

X-ray sources are the same for small-angle scattering as for crystallographic experiments. One can use conventional generators with sealed tubes or rotating anodes for higher power. For the vast majority of applications, an X-ray tube with copper anode is used; the wavelength of its characteristic radiation (Cu $K\alpha$ line) is 0.154 nm. Different anode materials emit X-rays of different characteristic wavelengths.

X-rays from synchrotrons or storage rings have a continuous wavelength distribution and the actual wavelength for the experiment is selected by a monochromator. The intensity is much higher than for any type of conventional source but synchrotron radiation is available only at a few places in the world. Reviews on synchrotron radiation and its application have been published during recent years (Stuhrmann, 1978; Holmes, 1982; Koch, 1988). In these reviews, one can also find some remarks on the general principles of the systems including cameras and special detectors.

2.6.1.5.1. *Small-angle cameras*

General. In any small-angle scattering experiment, it is necessary to illuminate the sample with a well defined flux of X-rays. The ideal condition would be a parallel monochromatic beam of negligible dimension and very high intensity. These theoretical conditions can never be reached in practice (Pessen, Kumosinski & Timasheff, 1973). One of the main reasons is the fact that there are no lenses as in the visible range of electromagnetic radiation. The refractive index of all materials is equal to or very close to unity for X-rays. On the other hand, this fact has some important advantages. It is, for example, possible to use circular capillaries as sample holders without deflecting the beam. There are different ways of constructing a small-angle scattering system. Slit, pinhole, and block systems define a certain area where the X-rays can pass. Any slit or edge will give rise to secondary scattering (parasitic scattering). The special construction of the instrument has to provide at least a subspace in the detector plane (plane of registration) that is free from this parasitic scattering. The crucial point is of course to provide the conditions to measure at very small scattering angles.

The other possibility of building a small-angle scattering system is to use monochromator crystals and/or bent mirrors to select a narrow wavelength band from the radiation (important for synchrotron radiation) and to focus the X-ray beam to a narrow spot. These systems require slits in addition to eliminate stray radiation.

Block collimation – Kratky camera. The Kratky (1982*a*) collimation system consists of an entrance slit (edge) and two blocks – the *U*-shaped centre piece and a block called *bridge*. With this system, the problem of parasitic scattering can be largely removed for the upper half of the plane of registration and the smallest accessible scattering angle is defined by the size of the entrance slit (see Fig. 2.6.1.13). This system can be integrated in an evacuated housing (Kratky compact camera) and fixed on the top of the X-ray tube. It is widely used in many laboratories for different applications. In the Kratky system, the X-ray beam has a rectangular shape, the length being much larger than the width. Instrumental broadening can be corrected by special numerical routines. The advantage is a relatively high primary-beam intensity. The main disadvantage is that it cannot be used in special applications such as oriented systems where

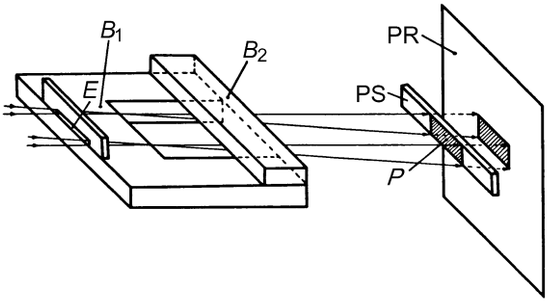

Fig. 2.6.1.13. Schematic drawing of the block collimation (Kratky camera): E edge; B_1 centre piece; B_2 bridge; P primary-beam profile; PS primary-beam stop; PR plane of registration.

the two-dimensional scattering pattern has to be recorded. For such applications, any type of point collimation can be used.

Slit and pinhole cameras. The simplest way to build a camera is to use two pairs of slits or pinholes at a certain distance apart (Kratky, 1982*a*; Holmes, 1982). The narrower the slits and the larger the distance between them, the smaller is the smallest attainable scattering angle (sometimes called the '*resolution*'). Parasitic scattering and difficult alignment are the main problems for all such systems (Guinier & Fournet, 1955). A slit camera that has been used very successfully is that of Beeman and co-workers (Ritland, Kaesberg & Beeman, 1950; Anderegg, Beeman, Shulman & Kaesberg, 1955). A rather unusual design is adopted in the slit camera of Stasiecki & Stuhrmann (1978), whose overall length is 50 m! A highly developed system is the ORNL 10 m camera at Oak Ridge (Hendricks, 1978).

Standard-size cameras for laboratory application are commercially available with different designs from various companies.

Bonse–Hart camera. The Bonse–Hart camera (Bonse & Hart, 1965, 1966, 1967) is based on multiple reflections of the primary beam from opposite sides of a groove in an ideal germanium crystal (collimator and monochromator). After penetrating the sample, the scattered beam runs through the groove of a second crystal (analyser). This selects the scattering angle. Rotation of the second crystal allows the measurement of the angle-dependent scattering function. The appealing feature of this design is that one can measure down to very small angles without a narrow entrance slit. The system is therefore favourable for the investigation of very large particles ($D > 350$ nm). For smaller particles, one obtains better results with block collimation (Kratky & Leopold, 1970).

Camera systems for synchrotron radiation. Small-angle scattering facilities at synchrotrons are built by the local staff and details of the construction are not important for the user in most cases. Descriptions of the instruments are available from the local contacts. These small-angle scattering systems are usually built with crystal monochromators and focusing mirrors (point collimation). All elements have to be operated under remote control for safety reasons. A review of the different instruments was published recently by Koch (1988).

2.6.1.5.2. *Detectors*

In this field, we are facing the same situation as we met for X-ray sources. The detectors for small-angle scattering experiments are the same as or slightly modified from the detectors used in crystallography. Therefore, it is sufficient to give a short summary of the detectors in the following; further details are given in Chapter 7.1. If we are not investigating the special cases of fully or partially oriented systems, we have to measure the dependence of the scattered intensity on the scattering angle, *i.e.* a one-dimensional function. This can be done with a standard gas-filled proportional counter that is operated in a sequential mode (Leopold, 1982), *i.e.* a positioning device moves the receiving slit and the detector to the desired angular position and the radiation detector senses the scattered intensity at that position. In order to obtain the whole scattering curve, a series of different angles must be positioned sequentially and the intensity readings at every position must be recorded. The system has a very high dynamic range, but – as the intensities at different angles are measured at different times – the stability of the primary beam is of great importance.

This drawback is eliminated in the parallel detection mode with the use of position-sensitive detectors. Such systems are in most cases proportional counters with sophisticated and expensive read-out electronics that can evaluate on-line the accurate position where the pulses have been created by the incoming radiation.

Two-dimensional position-sensitive detectors are necessary for oriented systems, but they also have advantages in the case of non-oriented samples when circular chambers are used or when integration techniques in square detectors lead to a higher signal at large scattering angles.

The simplest and cheapest two-dimensional detector is still film, but films are not used very frequently in small-angle scattering experiments because of limited linearity and dynamic range, and fog intensity.

Koch (1988) reviews the one- and two-dimensional detectors actually used in synchrotron small-angle scattering experiments. For a general review of detectors, see Hendrix (1985).

2.6.1.6. *Data evaluation and interpretation*

After having discussed the general principles and the basics of instrumentation in the previous subsections, we can now discuss how to handle measured data. This can only be a very short survey; a detailed description of data treatment and interpretation has been given previously (Glatter, 1982*a*,*b*).

Every physical investigation consists of three highly correlated parts: theory, experiment, and evaluation of data. The theory predicts a possible experiment, experimental data have to be collected in a way that the evaluation of the information wanted is possible, the experimental situation has to be described theoretically and has to be taken into account in the process of data evaluation *etc*. This correlation should be remembered at every stage of the investigation. Before we can start any discussion about interpretation, we have to describe the experimental situation carefully.

All the theoretical equations in the previous subsections correspond to ideal conditions as mentioned in the subsection on instrumentation. In real experiments, we do not measure with a point-like parallel and strictly monochromatic primary beam and our detector will have non-negligible dimensions. The finite size of the beam, its divergence, the size of the detector, and the wavelength distribution will lead to an instrumental broadening as in most physical investigations. The measured scattering curve is said to be *smeared* by these effects. So we find ourselves in the following situation.

The particle is represented by its PDDF $p(r)$. This function is not measured directly. In the scattering process it is Fourier-transformed into a scattering function $I(h)$ [equation (2.6.1.9)]. This function is smeared by the broadening effects and the final *smeared* scattering function $I_{\exp}(h)$ is measured with a certain experimental error $\sigma(h)$. In the case of polydisperse systems, the situation is very similar; we start from a size-distribution function $D(R)$ and have a different transformation [equations (2.6.1.54), (2.6.1.55)], but the smearing problem is the same.

2.6.1.6.1. *Primary data handling*

In order to obtain reliable results, we have to perform a series of experiments. We have to repeat the experiment for every sample, to be able to estimate a mean value and a standard deviation at every scattering angle. This experimentally determined standard deviation is often much higher than the standard deviation simply estimated from counting statistics. A blank experiment (cuvette filled with solvent only) is necessary to be able to subtract background scattering coming from the instrument and from the solvent (or *matrix* in the case of solid samples). Finally, we have to perform a series of such

experiments at different concentrations to extrapolate to zero concentration (elimination of interparticle interferences).

If the scattering efficiency of the sample is low (low contrast, small particles), it may be necessary to measure the outer part of the scattering function with a larger entrance slit and we will have to merge different parts of the scattering function. The intensity of the instrument (primary beam) should be checked before each measurement. This allows correction (normalization) for instabilities.

It is therefore necessary to have a so-called primary data-handling routine that performs all these preliminary steps like averaging, subtraction, normalization, overlapping, concentration extrapolation, and graphical representation on a graphics terminal or plotter. In addition, it is helpful to have the possibility of calculating the Guinier radius, Porod extrapolation [equations (2.6.1.24)], invariant, *etc*. from the raw data.

When all these preliminary steps have been performed, we have a smeared particle-scattering function $I_{\rm exp}(h)$ with a certain statistical accuracy. From this data set, we want to compute $I(h)$ and $p(r)$ [or $D(R)$] and all our particle parameters. In order to do this, we have to *smooth* and *desmear* our function $I_{\rm exp}(h)$. The smoothing operation is an absolute necessity because the desmearing process is comparable to a differentiation that is impossible for noisy data. Finally, we have to perform a Fourier transform (or other similar transformation) to invert equations (2.6.1.9) or (2.6.1.54), (2.6.1.55). Before we can discuss the desmearing process (collimation error correction) we have to describe the smearing process.

2.6.1.6.2. *Instrumental broadening – smearing*

These effects can be separated into three components: the two-dimensional geometrical effects and the wavelength effect. The geometrical effects can be separated into a slit-length (or slit-height) effect and a slit-width effect. The slit length is perpendicular to the direction of increasing scattering angle; the corresponding weighting function is usually called $P(t)$. The slit width is measured in the direction of increasing scattering angles and the weighting function is called $Q(x)$. If there is a wavelength distribution, we call the weighting function $W(\lambda')$ where $\lambda' = \lambda/\lambda_0$ and λ_0 is the reference wavelength used in equation (2.6.1.2). When a conventional X-ray source is used, it is sufficient in most cases to correct only for the $K\beta$ contribution. Instead of the weighting function $W(\lambda')$ one only needs the ratio between $K\beta$ and $K\alpha$ radiation, which has to be determined experimentally (Zipper, 1969). One or more smearing effects may be negligible, depending on the experimental situation.

Each effect can be described separately by an integral equation (Glatter, 1982*a*). The combined formula reads

$$\bar{I}_{\rm exp}(h) = 2 \int_{-\infty}^{\infty} \int_{0}^{\infty} \int_{0}^{\infty} Q(x)P(t)W(\lambda') \times I\left(\frac{[(m-x)^2 + t^2]^{1/2}}{\lambda'}\right) {\rm d}\lambda'\ {\rm d}t\ {\rm d}x. \qquad (2.6.1.56)$$

This threefold integral equation cannot be solved analytically. Numerical methods must be used for its solution.

2.6.1.6.3. *Smoothing, desmearing, and Fourier transformation*

There are many methods published that offer a solution for this problem. Most are referenced and some are reviewed in the textbooks (Glatter, 1982*a*; Feigin & Svergun, 1987). The *indirect transformation method* in its original version (Glatter, 1977*a*,*b*, 1980*a*,*b*) or in modifications for special applications (Moore, 1980; Feigin & Svergun, 1987) is a well established method used in the majority of laboratories for different applications. This procedure solves the problems of smoothing, desmearing, and Fourier transformation [inversion of equations (2.6.1.9) or (2.6.1.54), (2.6.1.55)] in one step. A short description of this technique is given in the following.

Indirect transformation methods. The *indirect transformation method* combines the following demands: single-step procedure, optimized general-function system, weighted least-squares approximation, minimization of termination effect, error propagation, and consideration of the physical smoothing condition given by the maximum intraparticle distance. This smoothing condition requires an estimate $D_{\rm max}$ as an upper limit for the largest particle dimension:

$$D_{\rm max} \geq D. \qquad (2.6.1.57)$$

For the following, it is not necessary for $D_{\rm max}$ to be a perfect estimate, but it must not be smaller than D.

As $p(r) = 0$ for $r \geq D_{\rm max}$, we can use a function system for the representation of $p(r)$ that is defined only in the subspace $0 \leq r \leq D_{\rm max}$. A linear combination

$$p_A(r) = \sum_{\nu=1}^{N} c_\nu \varphi_\nu(r) \qquad (2.6.1.58)$$

is used as an approximation to the PDDF. Let N be the number of functions and c_ν be the unknowns. The functions $\varphi_\nu(r)$ are chosen as cubic B splines (Greville, 1969; Schelten & Hossfeld, 1971) as they represent smooth curves with a minimum second derivative.

Now we take advantage of two facts. The first is that we know precisely how to calculate a smeared scattering function $\bar{I}(h)$ from $I(h)$ [equation (2.6.1.56)] and how $p(r)$ or $D(R)$ is transformed into $I(h)$ [equations (2.6.1.9) or (2.6.1.54), (2.6.1.55)], but we do not know the inverse transformations. The second fact is that all these transformations are linear, *i.e*. they can be applied to all terms in a sum like that in equation (2.6.1.58) separately. So it is easy to start with our approximation in real space [equation (2.6.1.58)] taking into account the *a priori* information $D_{\rm max}$. The approximation $I_A(h)$ to the ideal (unsmeared) scattering function can be written as

$$I_A(h) = \sum_{\nu=1}^{N} c_\nu \Psi_\nu(h), \qquad (2.6.1.59)$$

where the functions $\Psi_\nu(h)$ are calculated from $\varphi_\nu(r)$ by the transformations (2.6.1.9) or (2.6.1.54), (2.6.1.55), the coefficients c_ν remain unknown. The final fit in the smeared, experimental space is given by a similar series

$$\bar{I}_A(h) = \sum_{\nu=1}^{N} c_\nu \chi_\nu(h), \qquad (2.6.1.60)$$

where the $\chi_\nu(h)$ are functions calculated from $\psi_\nu(h)$ by the transform (2.6.1.56). Equations (2.6.1.58), (2.6.1.59), and (2.6.1.60) are similar because of the linearity of the transforms. We see that the functions $\chi_\nu(h)$ are calculated from $\varphi_\nu(r)$ in the same way as the data $\bar{I}_{\rm exp}(h)$ were produced by the experiment from $p(r)$. Now we can minimize the expression

$$L = \sum_{k=1}^{M} [\bar{I}_{\rm exp}(h_k) - \bar{I}_A(h_k)]^2 / \sigma^2(h_k), \qquad (2.6.1.61)$$

where M is the number of experimental points. Such *least-squares problems* are in most cases *ill conditioned, i.e*. additional stabilization routines are necessary to find the best

solution. This problem is far from being trivial, but it can be solved with standard routines (Glatter, 1977*a*,*b*; Tikhonov & Arsenin, 1977).

The whole process of data evaluation is shown in Fig. 2.6.1.14. Similar routines cannot be used in crystallography (periodic structures) because there exists no estimate for $D_{\max}$ [equation (2.6.1.57)].

Maximum particle dimension. The sampling theorem of Fourier transformation (Shannon & Weaver, 1949; Bracewell, 1986) gives a clear answer to the question of how the size of the particle D is related to the smallest scattering angle h_1. If the scattering curve is observed at increments $\Delta h \leq h_1$ starting from a scattering angle h_1, the scattering data contain, at least theoretically, the full information for all particles with maximum dimension D

$$D \leq \pi/h_1. \tag{2.6.1.62}$$

The first application of this theorem to the problem of data evaluation was given by Damaschun & Pürschel (1971*a*,*b*). In practice, one should always try to stay below this limit, *i.e.*

$$h_1 < \pi/D \quad \text{and} \quad \Delta h \ll h_1, \tag{2.6.1.63}$$

taking into account the loss of information due to counting statistics and smearing effects. An optimum value for $\Delta h = \pi/(6D)$ is claimed by Walter, Kranold & Becherer (1974).

Information content. The number of *independent* parameters contained in a small-angle scattering curve is given by

$$N_{\max} \leq h_2/h_1, \tag{2.6.1.64}$$

with h_1 and h_2 being the lower and upper limits of h. In practice, this limit certainly depends on the statistical accuracy of the data. It should be noted that the number of functions N in equations (2.6.1.58) to (2.6.1.60) may be larger than $N_{\max}$ because they are not independent. They are correlated by the stabilization routine. An example of this problem can be found in Glatter (1980*a*).

Resolution. There is no clear answer to the question concerning the smallest structural details, *i.e.* details in the $p(r)$ function that can be recognized from an experimental scattering function. The limiting factors are the maximum scattering angle h_2, the statistical error $\sigma(h)$, and the weighting functions $P(t)$, $Q(x)$, and $W(\lambda')$ (Glatter, 1982*a*). The resolution of standard experiments is not better than approximately 10% of the maximum dimension of the particle for a monodisperse system. In the case of polydisperse systems, resolution can be defined as the minimum relative peak distance that can be resolved in a bimodal distribution. We know from simulations that this value is of the order of 25%.

Special transforms. The PDDF $p(r)$ or the size distribution function $D(R)$ is related to $I(h)$ by equations (2.6.1.9) or (2.6.1.54), (2.6.1.55). In the special case of particles elongated in one direction (like cylinders), we can combine equations (2.6.1.41) and (2.6.1.43) and obtain

$$I(h) = 2\pi^2 L \int_0^\infty p_c(r) \frac{J_0(hr)}{h}\, \mathrm{d}r. \tag{2.6.1.65}$$

This Hankel transform can be used in the indirect transformation method for the calculation of $\psi_\nu(h)$ in (2.6.1.59). Doing this, we immediately obtain the PDDF of the cross section $p_c(r)$ from the smeared experimental data. It is not necessary to know the length L of the particle if the results are not needed on an absolute scale. For this application, we only need the information that the scatterers are elongated in one direction with a constant cross section. This information can be found from the overall PDDF of the particle or can be *a priori* information from other experiments, like electron microscopy. The estimate for the maximum dimension $D_{\max}$ (2.6.1.57) is related to the cross

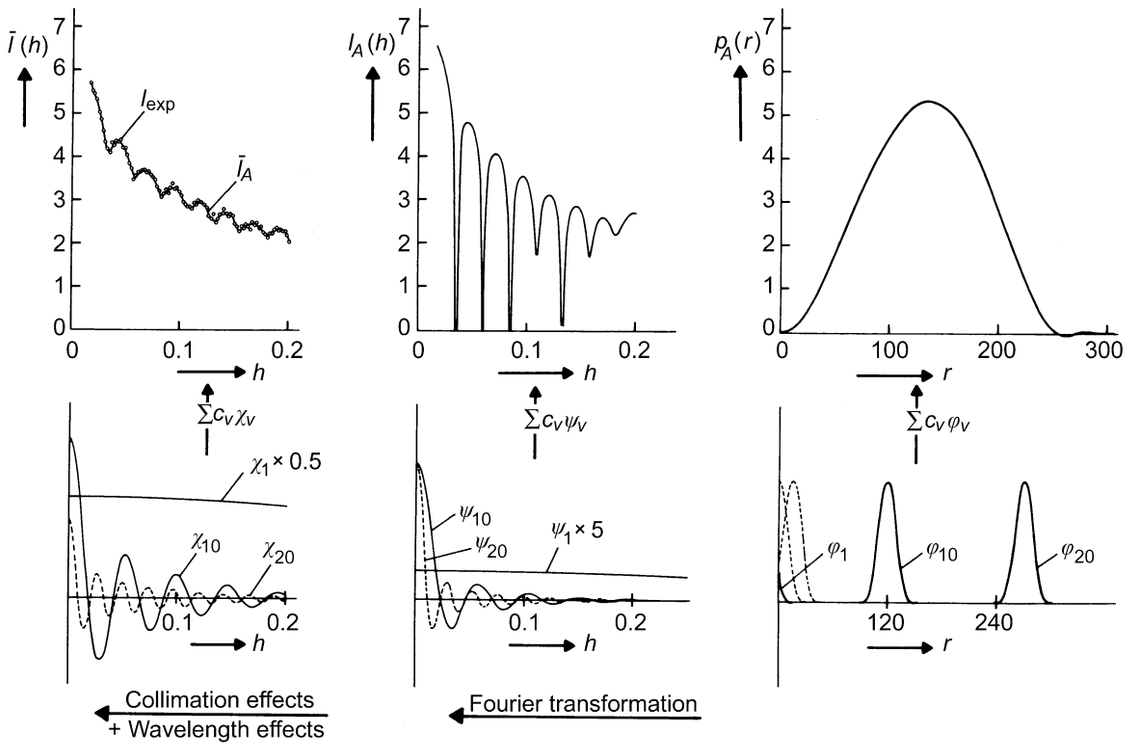

Fig. 2.6.1.14. Function systems $\varphi_\nu(r)$, $\Psi_\nu(h)$, and $\chi_\nu(h)$ used for the approximation of the scattering data in the indirect transformation method.

section in this application, *i.e.* the maximum dimension of the cross section must not be larger than $D_{\max}$.

The situation is quite similar for flat particles. If we combine (2.6.1.47) and (2.6.1.49), we obtain

$$I(h) = 4\pi A \int_0^\infty p_t(r) \frac{\cos(hr)}{h^2}\, \mathrm{d}r, \qquad (2.6.1.66)$$

$p_t(r)$ being the distance distribution function of the thickness. We have to check that the particles are flat with a constant thickness with maximum thickness $T \leq D_{\max}$. A is the area of the particles and would be needed only for experiments on an absolute scale.

2.6.1.6.4. *Direct structure analysis*

It is impossible to determine the three-dimensional structure $\rho(\mathbf{r})$ directly from the one-dimensional information $I(h)$ or $p(r)$. Any direct method needs additional *a priori information* – or assumptions – on the system under investigation. If this information tells us that the structure only depends on one variable, *i.e.* the structure is in a general sense *one dimensional*, we have a good chance of recovering the structure from our scattering data.

Examples for this case are particles with spherical symmetry, *i.e.* ρ depends only on the distance r from the centre, or particles with cylindrical or lamellar symmetry where ρ depends only on the distance from the cylinder axis or from the distance from the central plane in the lamella. We will restrict our discussion here to the spherical problem but we keep in mind that similar methods exist for the cylindrical and the lamellar case.

Spherical symmetry. This case is described by equations (2.6.1.51) and (2.6.1.52). As already mentioned in §2.6.1.3.2.2, we can solve the problem of the calculation of $\rho(r)$ from $I(h)$ in two different ways. We can calculate $\rho(r)$ *via* the distance distribution function $p(r)$ with a *convolution square-root* technique (Glatter, 1981; Glatter & Hainisch, 1984). The other way goes through the amplitude function $A(h)$ and its Fourier transform. In this case, one has to find the right phases (signs) in the square-root operation $\{A(h) = \pm[I(h)^{1/2}]\}$.The *box-function refinement* method by Svergun, Feigin & Schedrin (1984) is an iterative technique for the solution of the phase problem using the *a priori* information that $\rho(r)$ is equal to zero for $r \geq R_{\max}$ ($D_{\max}/2$). The same restriction is used in the convolution square-root technique. Under ideal conditions (perfect spherical symmetry), both methods give good results. In the case of deviations from spherical symmetry, one obtains better results with the convolution square-root technique (Glatter, 1988). With this method, the results are less distorted by non-spherical contributions.

Multipole expansions. A wide class of homogeneous particles can be represented by a boundary function that can be expanded into a series of spherical harmonics. The coefficients are related to the coefficients of a power series of the scattering function $I(h)$, which are connected with the moments of the PDDF (Stuhrmann, 1970*b*,*c*; Stuhrmann, Koch, Parfait, Haas, Ibel & Crichton, 1977). Of course, this expansion cannot be unique, *i.e.* for a certain scattering function $I(h)$ one can find a large variety of possible expansion coefficients and shapes. In any case, additional *a priori* information is necessary to reduce this number, which in turn influences the convergence of the expansion. Only compact, globular structures can be approximated with a small number of coefficients.

This concept is not restricted to the determination of the shape of the particles. Even inhomogeneous particles can be described using all possible radial terms in a general expansion (Stuhrmann, 1970*a*). The information content can be increased by contrast variation (Stuhrmann, 1982), but in any event one is left with the problem of how to find additional *a priori* information in order to reduce the possible structures. Any type of symmetry will lead to a considerable improvement. The case of axial symmetry is a good example. Svergun, Feigin & Schedrin (1982) have shown that the quality of the results can be further improved when upper and lower limits for $\rho(\mathbf{r})$ can be used. Such limits can come from a known chemical composition.

2.6.1.6.5. *Interpretation of results*

After having used all possible data-evaluation techniques, we end up with a desmeared scattering function $I(h)$, the PDDF $p(r)$ or the size-distribution function $D(R)$, and some special functions discussed in the previous subsections. Together with the particle parameters, we have a data set that can give us at least a rough classification of the substance under investigation.

The interpretation can be performed in reciprocal space (scattering function) or in real space (PDDF *etc*.). Any symmetry can be detected more easily in reciprocal space, but all other structural information can be found more easily in real space (Glatter, 1979, 1982*b*).

When a certain structure is estimated from the data and from *a priori* information, one has to test the corresponding model. That means one has to find the PDDF and $I(h)$ for the model and has to compare it with the experimental data. Every model that fits within the experimental errors can be true, all that do not fit have to be rejected. If the model does not fit, it has to be refined by trial and error. In most cases, this process is much easier in real space than in reciprocal space. Finally, we may end up with a set of possible structures that can be correct. Additional *a priori* information will be necessary to reduce this number.

2.6.1.7. *Simulations and model calculations*

2.6.1.7.1. *Simulations*

Simulations can help to find the limits of the method and to estimate the systematic errors introduced by the data-evaluation procedure. Simulations are performed with exactly known model systems (test functions). These systems should be similar to the structures of interest. The model data are transformed according to the special experimental situation (collimation profiles and wavelength distribution) starting from the theoretical PDDF (or scattering function). '*Experimental data points*' are generated by sampling in a limited h range and adding statistical noise from a random-number generator. If necessary, a certain amount of background scattering can also be added. This simulated data set is subjected to the data-evaluation procedure and the result is compared with the starting function. Such simulation can reveal the influence of each approximation applied in the various evaluation routines.

On the other hand, simulations can also be used for the optimization of the experimental design for a special application. The experiment situation is characterized by several contradictory effects: a large width for the functions $P(t)$, $Q(x)$, and $W(\lambda')$ leads to a high statistical accuracy but considerable smearing effects. The quality of the results of the desmearing procedure is increased by high statistical accuracy, but decreased by large smearing effects. Simulations can help to find the optimum for a special application.

2.6.1.7.2. *Model calculation*

In the section on data evaluation and interpretation, we have seen that we obtain a rough estimate for the structure of the particles under investigation directly from the experimental data. For further refinement, we have to compare our results with scattering functions or PDDF's from models

2.6.1.7.3. *Calculation of scattering intensities*

The scattering curves can be calculated semi-analytically for simple triaxial bodies and for models composed of some of these bodies. The scattering amplitude for regular bodies like ellipsoids, parallelepipeds, and cylinders can be calculated analytically for any orientation. The spatial averaging has to be performed numerically. Such calculations have been performed for a large number of different models by Porod (1948), Mittelbach & Porod (1961*a*,*b*, 1962), and by Mittelbach (1964). More complicated structures can be described by models composed of several such triaxial bodies, but the computing time necessary for such calculations can be hours on a mainframe computer.

Models composed only of spherical subunits can be evaluated with the Debye formula (Debye, 1915):

$$I(h) = i_{\rm el}(h) \sum_{i=1}^{N} \sum_{k=1}^{N} \rho_i V_i \rho_k V_k \Phi_i(h) \Phi_k(h) \frac{\sin(hd_{ik})}{hd_{ik}}, \quad (2.6.1.67)$$

where the spatial average is carried out analytically. Another possibility would be to use spherical harmonics as discussed in the previous section but the problem is how to find the expansion coefficients for a certain given geometrical structure.

2.6.1.7.4. *Method of finite elements*

Models of arbitrary shape can be approximated by a large number of very small homogeneous elements of variable electron density. These elements have to be smaller than the smallest structural detail of interest.

Sphere method. In this method, the elements consist of spheres of equal size. The diameter of these spheres must be chosen independently of the distance between nearest neighbours, in such a way that the total volume of the model is represented correctly by the sum of all volume elements (which corresponds to a slight formal overlap between adjacent spheres). The scattering intensity is calculated using the Debye formula (2.6.1.67), with $\Phi_i(h) = \Phi_k(h) = \Phi(h)$.

The computing time is mainly controlled by the number of mutual distances between the elements. The computing time can be lowered drastically by the use of approximate d_{ik} values in (2.6.1.67). Negligible errors in $I(h)$ result if d_{ik} values are quantized to $D_{\max}/10000$ (Glatter, 1980*c*). For the practical application (input operation), it is important that a certain number of elements can be combined to form so-called substructures that can be used in different positions with arbitrary weights and orientations to build the model.

The sphere method can also be used for the computation of scattering curves for macromolecules from a known crystal structure. The weights of the atoms are given by the effective number of electrons

$$Z_{\rm eff} = Z - \rho_0 V_{\rm eff}, \quad (2.6.1.68)$$

where $V_{\rm eff}$ is the apparent volume of the atom given by Langridge, Marvin, Seeds, Wilson, Cooper, Wilkins & Hamilton (1960).

Cube method. This method has been developed independently by Fedorov, Ptitsyn & Voronin (1972, 1974*a*,*b*) and by Ninio & Luzzati (1972) mainly for the computation of scattered intensities for macromolecules in solution whose crystal structure is known. In the cube method, the macromolecule is mentally placed in a parallelepiped, which is subdivided into small cubes (with edge lengths of 0.5–1.5 Å. Each cube is examined in order to decide whether it belongs to the molecule or to the solvent. Adjacent cubes in the z direction are joined to form parallelepipeds. The total scattering amplitude is the sum over the amplitudes from the parallelepipeds with different positions and lengths. The mathematical background is described by Fedorov, Ptitsyn & Voronin (1974*a*,*b*). The *modified cube method* of Fedorov & Denesyuk (1978) takes into account the possible penetration of the molecule by water molecules.

2.6.1.7.5. *Calculation of distance-distribution functions*

The PDDF can be calculated analytically only for a few simple models (Porod, 1948; Goodisman, 1980); in all other cases, we have to use a finite element method with spheres. It is possible to define an analogous equation to the Debye formula (2.6.1.67) in real space (Glatter, 1980*c*). The PDDF can be expressed as

$$p(r) = \sum_{i=1}^{N} \rho_i^2 p_0(r, R_i) + 2 \sum_{i=1}^{N-1} \sum_{k=i+1}^{N} \rho_i \rho_k p(r, d_{ik}, R_i, R_k). \quad (2.6.1.69)$$

$p_0(r, R_i)$ is the PDDF of a sphere with radius R_i and electron density equal to unity, $p(r, d_{ik}, R_i, R_k)$ is the cross-term distance distribution between the ith and kth spheres (radii R_i and R_k) with a mutal distance d_{ik}.

Equation (2.6.1.69) [and (2.6.1.67)] can be used in two different ways for the calculation of model functions. Sometimes, it is possible to approximate a macromolecule as an aggregate of some spheres of well defined size representing different globular subunits (Pilz, Glatter, Kratky & Moring-Claesson, 1972). The form factors of the subunits are in such cases real parameters of the model. However, in most cases we have no such possibility and we have to use the method of finite elements, *i.e.* we fit our model with a large number of sufficiently small spheres of equal size, and, if necessary, different weight. The form factor of the small spheres is now not a real model parameter and introduces a limit of resolution.

Fourier transformation [equation (2.6.1.10)] can be used for the computation of the PDDF of any arbitrary model if the scattering function of the model is known over a sufficiently large range of h values.

2.6.1.8. *Suggestions for further reading*

Only a few textbooks exist in the field of small-angle scattering. The classic monograph *Small-Angle Scattering of X-rays* by Gunier & Fournet (1955) was followed by the proceedings of the conference at Syracuse University, 1965, edited by Brumberger (1967) and by *Small-Angle X-ray Scattering* edited by Glatter & Kratky (1982). The several sections of this book are written by different authors being experts in the field and representing the state of the art at the beginning of the 1980's. The monograph *Structure Analysis by Small-Angle X-ray and Neutron Scattering* by Feigin & Svergun (1987) combines X-ray and neutron techniques.

2.6.2. Neutron techniques (By R. May)

Symbols used in the text

A	sample area
A_s	inner sample surface
b_i	coherent scattering length of atom i
B_i	spin-dependent scattering length of atom i
C	sample concentration in g l^{-1}
c	volume fraction occupied by matter
d	sample thickness
D	particle dimension
DCD	double-crystal diffractometer
d_0	Bragg spacing
$\mathbf{e}$, $\mathbf{e}_0$	unit vectors along the diffracted and incident beams
$\mathbf{I}$	nuclear spin
IFT	indirect Fourier transformation
N	number of particles in the sample
N_A	Avogadro's number
Q	momentum transfer [$= (4\pi/\lambda)\sin\theta$]
r	radius of a sphere
R_G	radius of gyration
$\mathbf{s}$	neutron spin
SANS	small-angle neutron scattering
SAXS	small-angle X-ray scattering
T	transmission
TOF	time of flight
v	partial specific volume
V_p	particle volume
V_s	sample volume
$\Delta\Omega$	solid angle subtended by a detection element
λ	wavelength
ρ	scattering-length density
2θ	full scattering angle
$\mathrm{d}\sigma(Q)/\mathrm{d}\Omega$	scattering cross section per particle and unit solid angle

2.6.2.1. *Relation of X-ray and neutron small-angle scattering*

X-ray and neutron small-angle scattering (SAXS and SANS, respectively) are dealing with the same family of problems, *i.e.* the investigation of 'inhomogeneities' in matter. These inhomogeneities have dimensions D of the order of 1 to 100 nm, which are larger than interatomic distances, *i.e.* 0.3 nm. The term inhomogeneities may mean clusters in metals, a small concentration of protonated chains in an otherwise identical deuterated polymer – or *vice versa* – but also particles as well defined as purified proteins in aqueous solution.

In most cases, the inhomogeneities are not ordered. This is where small-angle scattering is most useful: many systems are not crystalline, cannot be crystallized, or do not exhibit the same properties if they are. One field, if one may say so, of SANS where samples are ordered is low-resolution crystallography of biological macromolecules. It will not be treated further here. In the case of crystalline order, the scattering of the single particle is observed with an amplification factor of N^2 for N identical particles in the crystal, but only for those scattering vectors observing the Bragg condition $n\lambda = 2d_0\sin\theta$. For disordered, randomly oriented particles, the amplification is only N, and the scattering pattern is lacking all information on particle orientation. Moreover, the real-space information on the internal arrangement of atoms within the inhomogeneities is reduced to the 'distance distribution function', a sine Fourier transform of the scattering intensity.

The mathematical descriptions of SAXS and SANS are either identical or hold with equivalent terms. The reader is referred to Section 2.6.1 on X-ray small-angle scattering techniques for a general description of low-Q scattering. An abundant treatment of SAXS can be found in the book edited by Glatter & Kratky (1982), and in Guinier & Fournet (1955) and Guinier (1968). A general introduction to SANS is given, for example, by Kostorz (1979) and by Hayter (1985). This section deals mainly with the differences between the techniques.

Altogether, neutrons are used for low-Q scattering essentially for the same reasons as for other neutron experiments. These reasons are:

(1) neutrons are sensitive to the isotopic composition of the sample;

(2) neutrons possess a magnetic moment and, therefore, can be used as a magnetic probe of the sample; and

(3) because of their weak interaction with and consequent deep penetration into matter, neutrons allow us to investigate properties of the bulk;

(4) for similar reasons, strong transparent materials are available as sample-environment equipment.

The fact that the kinetic energies of thermal and cold neutrons are comparable to those of excitations in solids, which is a reason for the use of neutrons for inelastic scattering, is, with the exception of time-of-flight SANS (see §2.6.2.1.1), not of importance for SANS.

The information obtained from low-Q scattering is always an average over the irradiated sample volume and over time. This average may be purely static (in the case of solids) or also dynamic (liquids). The limited Q range used does not resolve interatomic scattering contributions. Thus, a 'scattering-length density' ρ can be introduced, $\rho = \sum b_i/V$, where b_i are the (coherent) scattering lengths of the atoms within a volume V with linear dimensions of at least λ/π. Inhomogeneities can then be understood as regions where the scattering-length density deviates from the prevailing average value.

2.6.2.1.1. *Wavelength*

In the case of SANS – as in that of X-rays from synchrotron sources – the wavelength dependence of the momentum transfer Q, $Q = (4\pi/\lambda)\sin\theta$, where θ is half the scattering angle and λ is the wavelength, has to be taken into account explicitly. Q corresponds to k, h, and $2\pi s$ used by other authors.

SANS offers an optimal choice of the wavelength: with sufficiently large wavelengths, for example, first-order Bragg scattering (and therefore the contribution of multiple Bragg scattering to small-angle scattering) can be suppressed: The Bragg condition written as $\lambda/d_{\max} = (2\sin\theta)/n < 2$ cannot hold for $\lambda \geq 2d_{\max}$, where $d_{\max}$ is the largest atomic distance in a crystalline sample. For the usually small scattering angles in SANS, even quite small λ will not produce first-order peaks.

The neutrons produced by the fuel element of a reactor or by a pulsed source are moderated by the (heavy) water surrounding the core. Normally, the neutrons leave the reactor with a thermal velocity distribution. Cold sources, small vessels filled with liquid deuterium in the reactor tank, permit the neutron velocity distribution to be slowed down ('cold' neutrons) and lead to neutron wavelengths (range 0.4 to 2 nm) which are more useful for SANS.

At reactors, a narrow wavelength band is usually selected for SANS either by an artificial-multilayer monochromator or – more frequently, owing to the slow speed of cold neutrons – by a velocity selector. This is a rotating drum with a large number (about 100) of helical slots at its circumference, situated at the entrance of the neutron guides used for collimation. Only neutrons of the suitable velocity are able to pass through this

drum. The wavelength resolution $\Delta\lambda/\lambda$ of velocity selectors is usually between 5 and 40% (full width at half-maximum, FWHM); 10 and 20% are frequently used values.

Alternatively, time-of-flight (TOF) SANS cameras have been developed on pulsed neutron sources (*e.g.* Hjelm, 1988). These use short bunches (about 100 μs long) of neutrons with a 'white' wavelength spectrum produced by a pulsed high-energy proton beam impinging on a target with a repetition rate of the order of 10 ms. The wavelength and, consequently, the Q value of a scattered neutron is determined by its flight time, if the scattering is assumed to be quasi-elastic. The dynamic Q range of TOF SANS instruments is rather large, especially in the high-Q limit, owing to the large number of rapid neutrons in the pulse. The low-Q limit is determined by the pulse-repetition rate of the source because of frame overlap with the following pulse. It can be decreased, if necessary with choppers turning in phase with the pulse production and selecting only every nth pulse. This disadvantage does not exist for reactor-based TOF SANS cameras, where the pulse-repetition rate can be optimally adapted to the chosen maximal and minimal wavelength. A principal problem for TOF SANS exists in the 'upscattering' of cold neutrons, *i.e.* their gain in energy, by ^{1}H-rich samples: The background scattering may not arrive simultaneously with the elastic signal, and may thus not be attributed to the correct Q value (Hjelm, 1988).

2.6.2.1.2. *Geometry*

With typical neutron wavelengths, low Q need not necessarily mean small angles: The interesting Q range for an inhomogeneity of dimension D can be estimated as $1/D < Q < 10/D$. The scattering angle corresponding to the upper Q limit for $D = 10$ nm is 1.4° for Cu $K\alpha$ radiation, but amounts to 9.1° for neutrons of 10 nm wavelength. Consequently, it is preferable to speak of low-Q rather than of small-angle neutron scattering.

'Pin-hole'-type cameras are the most frequently used SANS instruments; an example is the SANS camera D11 at the Institut Max von Laue–Paul Langevin in Grenoble, France (Ibel, 1976; Lindner, May & Timmins, 1992), from which some of the numbers below are quoted. Since the cross section of the primary beam is usually chosen to be rather large (*e.g.* 3×5 cm) for intensity reasons, pin-hole instruments tend to be large. The smallest Q value that can be measured at a given distance is just outside the image of the direct beam on the detector (which either has to be attenuated or is hidden behind a beamstop, a neutron-absorbing plate of several 10 cm^2, *e.g.* of cadmium). Very small Q values thus require long sample-to-detector distances. The area detector of D11, with a surface of 64×64 cm and resolution elements of 1 cm^2, moves within an evacuated tube of 1.6 m diameter and a length of 40 m. Thus, a Q range of 5×10^{-3} to 5 nm^{-1} is covered. The geometrical resolution is determined by the length of the free neutron flight path in front of the sample, moving sections of neutron guide into or out of the beam ('collimation'). In general, the collimation length is chosen roughly equal to the sample-to-detector distance. Thus, the geometrical and wavelength contributions to the Q resolution match at a certain distance of the scattered beam from the direct-beam position in the detector plane. In order to resolve scattering patterns with very detailed features, *e.g.* of particles with high symmetry, longer collimation lengths are sometimes required at the expense of intensity.

Much more compact double-crystal neutron diffractometers [described for X-rays by Bonse & Hart (1966)] are being used to reach the very small Q values of some 10^{-4} nm^{-1} typical of static light scattering. The sample is placed between two crystals. The first crystal defines the wavelength and the direction of the incoming beam. The other crystal scans the scattered intensity. The resolution of such an instrument is mainly determined by the Darwin widths of the ideal crystals. This fact is reflected in the low neutron yield. Slit geometry can be used, but not 2D detectors.

A recent development is the ellipsoidal-mirror SANS camera. The mirror, which needs to be of very high surface quality, focuses the divergent beam from a small (several mm^2) source through the sample onto a detector with a resolution of the order of 1×1 mm. Owing to the more compact beam image, all other dimensions of the SANS camera can be reduced drastically (Alefeld, Schwahn & Springer, 1989). Whether or not there is a gain in intensity as compared with pin-hole geometry is strongly determined by the maximal sample dimensions. Long mirror with cameras (*e.g.* 20 m) are always superior to double-crystal instruments in this respect (Alefeld, Schwahn & Springer, 1989), and can also reach the light-scattering Q domain ($Q_{\min}$ of some 10^{-4} nm^{-1}, corresponding to particles of several μm dimension).

2.6.2.1.3. *Correction of wavelength, slit, and detector-element effects*

Resolution errors affect SANS data in the same way as X-ray scattering data, for which one may find a detailed treatment in an article by Glatter (1982*b*); there is one exception to this; namely, gravity, which of course only concerns neutron scattering, and only in rare cases (Boothroyd, 1989). Since SANS cameras usually work with pin-hole geometry, the influences of the slit sizes, *i.e.* the effective source dimensions, on the scattering pattern are small; even less important is, in general, the pixel size of 2D detectors. The preponderant contribution to the resolution of the neutron-scattering pattern is the wavelength-distribution function after the monochromatizing device, especially at larger angles. The situation is more complicated for TOF SANS (Hjelm, 1988).

As has been shown in an analytical treatment of the resolution function by Pedersen, Posselt & Mortensen (1990), who also quote some relevant references, resolution effects have a small influence on the results of the data analysis for scattering patterns with a smooth intensity variation and without sharp features. Therefore, one may assume that a majority of SANS patterns are not subjected to desmearing procedures.

Resolution has to be considered for scattering patterns with distinct features, as from spherical latex particles (Wignall, Christen & Ramakrishnan, 1988) or from viruses (Cusack, 1984). Size-distribution and wavelength-smearing effects are similar; it is evident that wavelength effects have to be corrected for if the size distribution is to be obtained.

Since measured scattering curves contain errors and have to be smoothed before they can be desmeared, iterative indirect methods are, in general, superior: A guessed solution of the scattering curve is convoluted with known smearing parameters and iteratively fitted to the data by a least-squares procedure. The guessed solution can be a simply parameterized scattering curve, without knowledge of the sample (Schelten & Hossfeld, 1971), but it is of more interest to fit the smeared Fourier transform of the distance-distribution function (Glatter, 1979) or the radial density distribution (*e.g.* Cusack, Mellema, Krijgsman & Miller, 1981) of a real-space model to the data.

2.6.2.2. *Isotopic composition of the sample*

Unlike X-rays, which 'see' the electron clouds of atoms within a sample, neutrons interact with the point-like nuclei. Since their

form factor does not decay like the atomic form factor, an isotropic background from the nuclei is present in all SANS measurements.

While X-ray scattering amplitudes increase regularly with the atomic number, neutron coherent-scattering amplitudes that give rise to the interference scattering necessary for structural investigations vary irregularly (see Bacon, 1975). Isotopes of the same element often have considerably different amplitudes owing to their different resonant scattering. The most prominent example of this is the difference of the two stable isotopes of hydrogen, ^{1}H and ^{2}H (deuterium). The coherent-scattering length of ^{2}H is positive and of similar value to that of most other elements in organic matter, whereas that of ^{1}H is negative, *i.e.* for ^{1}H there is a 180° phase shift of the scattered neutrons with respect to other nuclei.

This latter difference has been exploited vastly in the fields of polymer science (*e.g.* Wignall, 1987) and structural molecular biology (*e.g.* Timmins & Zaccai, 1988), in mainly two complementary respects, contrast variation and specific isotopic labelling.

In the metallurgy field, other isotopes are being used frequently for similar purposes, for example the nickel isotope ^{62}Ni, which has a negative scattering length, and the silver isotopes ^{107}Ag and ^{109}Ag (see the review of Kostorz, 1988).

2.6.2.2.1. *Contrast variation*

The easiest way of using the scattering-amplitude difference between ^{1}H and ^{2}H is the so-called contrast variation. It was introduced into SANS by Ibel & Stuhrmann (1975) on the basis of X-ray crystallographic (Bragg & Perutz, 1952), SAXS (Stuhrmann & Kirste, 1965), and light-scattering (Benoit & Wippler, 1960) work. Most frequently, contrast variation is carried out with mixtures of light (^1H_2O) and heavy water (^2H_2O), but also with other solvents available in protonated and deuterated form (ethanol, cyclohexane, *etc.*). The scattering-length density of H_2O varies between -0.562×10^{10} cm^{-2} for normal water, which is nearly pure ^1H_2O, and 6.404×10^{10} cm^{-2} for pure heavy water.

The scattering-length densities of other molecules, in general, are different from each other and from pure protonated and deuterated solvents and can be matched by ^{1}H/^{2}H mixture ratios characteristic for their chemical compositions. This mixture ratio (or the corresponding absolute scattering-length density) is called the scattering-length-density match point, or, semantically incorrect, contrast match point. If a molecule contains non-covalently bound hydrogens, they can be exchanged for solvent hydrogens. This exchange is proportional to the ratio of all labile ^{1}H and ^{2}H present; in dilute aqueous solutions, it is dominated by the solvent hydrogens. A plot of the scattering-length density *versus* the ^{2}H/(^{2}H+^{1}H) ratio in the solvent shows a linear increase if there is exchange; the value of the match point also depends on solvent exchange. The fact that many particles have high contrast with respect to ^2H_2O makes neutrons superior to X-rays for studying small particles at low concentrations.

The scattered neutron intensity from N identical particles without long-range interactions in a (very) dilute solution with solvent scattering density ρ_s can be written as

$$I(Q) = [\mathrm{d}\sigma(Q)/\mathrm{d}\Omega]NTAI_0\Delta\Omega, \qquad (2.6.2.1)$$

with the scattering cross section per particle and unit solid angle

$$\mathrm{d}\sigma(Q)/\mathrm{d}\Omega = \left\langle \left| \int [\rho(\mathbf{r}) - \rho_s] \exp(i\mathbf{Q}\cdot\mathbf{r})\, \mathrm{d}\mathbf{r} \right|^2 \right\rangle. \qquad (2.6.2.1a)$$

The angle brackets indicate averaging over all particle orientations. With $\rho(r) = \sum b_i/V_p$ and $I(0) = \text{constant} \times \left\langle \left| \int [\rho(\mathbf{r}) - \rho_s]\, \mathrm{d}\mathbf{r} \right|^2 \right\rangle$, we find that the scattering intensity at zero angle is proportional to

$$\Delta\rho = \sum b_i/V_p - \rho_s, \qquad (2.6.2.2)$$

which is called the contrast. The exact meaning of V_p is discussed, for example, by Zaccai & Jacrot (1983), and for X-rays by Luzzati, Tardieu, Mateu & Stuhrmann (1976).

The scattering-length density $\rho(\mathbf{r})$ can be written as a sum

$$\rho(\mathbf{r}) = \rho_0 + \rho_F(\mathbf{r}), \qquad (2.6.2.3)$$

where ρ_0 is the average scattering-length density of the particle at zero contrast, $\Delta\rho = 0$, and $\rho_F(\mathbf{r})$ describes the fluctuations about this mean. $I(Q)$ can then be written

$$I(Q) = (\rho_0 - \rho_2)^2 I_c(Q) + (\rho_0 - \rho_s) I_{cs}(Q) + I_s(Q). \qquad (2.6.2.4)$$

I_s is the scattering intensity due to the fluctuations at zero contrast. The cross term $I_{cs}(Q)$ also has to take account of solvent-exchange phenomena in the widest sense (including solvent water molecules bound to the particle surface, which can have a density different from that of bulk water). This extension is mathematically correct, since one can assume that solvent exchange is proportional to $\Delta\rho$. The term I_c is due to the invariant volume inside which the scattering density is independent of the solvent (Luzzati, Tardieu, Mateu & Stuhrmann, 1976). This is usually not the scattering of a homogeneous particle at infinte contrast, if the exchange is not uniform over the whole particle volume, as is often the case, or if the particle can be imaged as a sponge (see Witz, 1983).

The method is still very valuable, since it allows calculation of the scattering at any given contrast on the basis of at least three measurements at well chosen ^{1}H/^{2}H ratios (including data near, but preferentially not exactly at, the lowest contrasts). It is sometimes limited by ^{2}H-dependent aggregation effects.

2.6.2.2.2. *Specific isotopic labelling*

Specific isotope labelling is a method that has created unique applications of SANS, especially in the polymer field. Again, it is mainly concerned with the exchange of ^{1}H by ^{2}H, this time in the particles to be studied themselves, at hydrogen positions that are not affected by exchange with solvent atoms, for example carbon-bound hydrogen sites.

With this technique, isolated polymer chains can be studied in the environment of other polymer chains which are identical except for the hydrogen atoms, which are either ^{1}H or ^{2}H. Even if some care has to be taken as far as slightly modified thermodynamics are concerned, there is no other method that could replace neutrons in this field.

Inverse contrast variation forms an intermediate between the two methods described above. The contrast with respect to the solvent of a whole particle or of well defined components of a particle, for example a macromolecular complex, is changed by varying its degree of deuteration. That of the solvent remains constant. Since solvent-exchange effects remain practically identical for all samples, the measurements can be more precise than in the classical contrast variation (Knoll, Schmidt & Ibel, 1985).

2.6.2.3. *Magnetic properties of the neutron*

Since the neutron possesses a magnetic moment, it is sensitive to the orientation of spins in the sample [see, for example, Abragam *et al.* (1982)]. Especially in the absence of any other (isotopic) contrast, an inhomogeneous distribution of spins in the

sample is detectable by neutron low-Q scattering. The neutron spins need not be oriented themselves, although important contributions can be expected from measuring the difference between the scattering of neutron beams with opposite spin orientation. At present, several low-Q instruments are being planned or even built including neutron polarization and polarization analysis.

Studies of magnetic SANS without (and rarely with) neutron polarization include dislocations in magnetic crystals and amorphous ferromagnets [see the review of Kostorz (1988)].

Janot & George (1985) have pointed out that it is important to apply contrast variation for suppressing surface-roughness scattering and/or volume scattering in order to isolate magnetic scattering contributions by matching the scattering-length density of the material with that of a mixture of heavy and light water or oil, *etc*.

2.6.2.3.1. *Spin-contrast variation*

For a long time, the magnetic properties of the neutron have been neglected as far as 'nonmagnetic' matter is concerned. Spin-contrast variation, proposed by Stuhrmann (Stuhrmann *et al.*, 1986; Knop *et al.*, 1986), takes advantage of the different scattering lengths of the hydrogen atoms in its spin-up and spin-down states. Normally, these two states are mixed, and the cross section of unpolarized neutrons with the undirected spins gives rise to the usual value of the scattering amplitude of hydrogen. If, however, one is able to orient the spins of a given atom, and especially hydrogen, then the interaction of *polarized* neutrons with the two different oriented states offers an important contribution to the scattering amplitude:

$$A = b + 2B\mathbf{I} \cdot \mathbf{s}, \qquad (2.6.2.5)$$

where b is the isotropic nuclear scattering amplitude, B is the spin-dependent scattering amplitude, $\mathbf{s}$ is the neutron spin, and $\mathbf{I}$ the nuclear spin. For hydrogen, $b = -0.374 \times 10^{-12}$ cm, $B = 2.9 \times 10^{-12}$ cm.

The sample protons are polarized at very low temperatures (order of mK) and high magnetic fields (several tesla) by dynamic nuclear polarization, *i.e.* by spin–spin coupling with the electron spins of a paramagnetic metallo-organic compound present in the sample, which are polarized by a resonant microwave frequency. It is clear that the principles mentioned above also apply to other than biological and chemical material.

2.6.2.4. *Long wavelengths*

An important aspect of neutron scattering is the ease of using long wavelengths: Long-wavelength X-rays are produced efficiently only by synchrotrons, and therefore their cost is similar to that of neutrons. Unlike neutrons, however, they suffer from their strong interaction with matter. This disadvantage, which is acceptable with the commonly used Cu $K\alpha$ radiation, is in most cases prohibitive for wavelengths of the order of 1 nm.

Very low Q values are more easily obtained with long wavelengths than with very small angles, as is necessary with X-rays, since the same Q value can be observed further away from the direct beam. Objects of linear dimensions of several 100 nm, *e.g.* opals, where spherical particles of amorphous silica form a close-packed lattice with cell dimensions of up to several hundreds of nm, can still be investigated easily with neutrons. X-ray double-crystal diffractometers (Bonse & Hart, 1966), which may also reach very low Q, are subject to transmission problems, and neutron DCD's again perform better.

2.6.2.5. *Sample environment*

Important new fields of low-Q scattering, such as dynamic studies of polymers in a shear gradient and time-resolved studies of samples under periodic stress or under high pressure, have become accessible by neutron scattering because the weak interaction of neutrons with (homogeneous) matter permits the use of relatively thick (several mm) sample container walls, for example of cryostats, Couette-type shearing apparatus (Lindner & Oberthür, 1985, 1988), and ovens. Air scattering is not prohibitive, and easy-to-handle standard quartz cells serve as sample containers rather than very thin ones with mica windows in the case of X-rays.

Unlike with X-rays, samples can be relatively thick, and nevertheless be studied to low Q values. This is particularly evident for metals, where X-rays are usually restricted to thin foils, but neutrons can easily accept samples 1–10 mm thick.

2.6.2.6. *Incoherent scattering*

Incoherent scattering is produced by the interaction of neutrons with nuclei that are not in a fixed phase relation with that of other nuclei. It arises, for example, when molecules do not all contain the same isotope of an element (isotopic incoherent scattering). The most important source of incoherent scattering in SANS, however, is the spin-incoherent scattering from protons. It results from the fact that only protons and neutrons with identical spin directions can form an intermediate compound nucleus. The statistical probabilities of the parallel and antiparallel spin orientations, the similarity in size of the scattering lengths for spin up and spin down and their opposite sign result in an extremely large incoherent scattering cross section for ^{1}H, together with a coherent cross section of normal magnitude (but negative sign). Incoherent scattering contributes a background that can be by orders of magnitude more important than the coherent signal, especially at larger Q. On the other hand, it can be used for the calibration of the incoming intensity and of the detector efficiency (see below).

2.6.2.6.1. *Absolute scaling*

Wignall & Bates (1987) compare many different methods of absolute calibration of SANS data. Since the scattering from a thin water sample is frequently already being used for correcting the detector response [see §2.6.2.6.2], there is an evident advantage for performing the absolute calibration by H_2O scattering.

For a purely isotropic scatterer, the intensity scattered into a detector element of surface ΔA spanning a solid angle $\delta\Omega = \Delta A/4\pi L^2$ can be expressed as

$$\Delta I = I_0(1 - T_i)\delta\Omega g/4\pi, \qquad (2.6.2.6)$$

with T_i the transmission of the isotropic scatterer, *i.e.* the relation of the number of neutrons in the primary beam measured within a time interval Δt after having passed through the sample, I_{Tr}, and the number of neutrons I_0 observed within Δt without the sample. In practice, T_i is measured with an attenuated beam; typical attenuation factors are about 100 to 1000. g is a geometrical factor taking into account the sample surface and the solid angle subtended by the apparent source, *i.e.* the cross section of the neutron guide exit.

Vanadium is an incoherent scatterer frequently used for absolute scaling. Its scattering cross section, however, is more than an order of magnitude lower than that of protons. Moreover, the surface of vanadium samples has to be handled with much care in order to avoid important contributions from

surface scattering by scratches. The vanadium sample has to be hermetically sealed to prevent hydrogen incorporation (Wignall & Bates, 1987).

The coherent cross sections of the two protons and one oxygen in light water add up to a nearly vanishing *coherent*-scattering-length density, whereas the incoherent scattering length of the water molecule remains very high. The (quasi)isotropic incoherent scattering from a thin, *i.e.* about 1 mm or less, sample of ^1H_2O, therefore, is an ideal means for determining the absolute intensity of the sample scattering (Jacrot, 1976; Stuhrmann *et al.*, 1976), on condition that the sample-to-detector distance L is not too large, *i.e.* up to about 10 m. A function $f(\sigma_t[H_2O], \lambda)$ that accounts for deviations from the isotropic behaviour due to inelastic incoherent-scattering contributions of ^1H_2O and for the influence of the wavelength dependence of the detector response has to be multiplied to the right-hand side of equation (2.6.2.6) (May, Ibel & Haas, 1982). f can be determined experimentally and takes values of around 1 for wavelengths around 1 nm.

Since the intensity scattered into a solid angle $\Delta\Omega$ is

$$I(Q) = P(Q)NT_sI_0g\left(\sum b_i - \rho_sV\right)^2, \qquad (2.6.2.7)$$

where $P(Q)$ is the form factor of the scattering of one particle, and the geometrical factor g can be chosen so that it is the same as that of equation (2.6.2.6) (same sample thickness and surface and identical collimation conditions), we obtain

$$I(Q) = 4\pi P(Q)NT_sf(\sigma_t[H_2O], \lambda)\left(\sum b_i - \rho_sV\right)^2/(1 - T[H_2O]). \qquad (2.6.2.8)$$

Note that the scattering intensities mentioned above are scattering intensities corrected for container scattering, electronic and neutron background noise, and, in the case of the sample, for the solvent scattering.

2.6.2.6.2. *Detector-response correction*

For geometrical reasons (*e.g.* sample absorption), and in the case of 2D detectors also for electronic reasons, the scattering curves cannot be measured with a sensitivity uniform over all the angular region. Therefore, the scattering curve has to be corrected by that of a sample with identical geometrical properties, but scattering the neutrons with the same probability into all angles (at least in the forward direction). As we have seen previously, such samples are vanadium and thin cells filled with light water. Again, water has the advantage of a much higher scattering cross section, and is less influenced by surface effects.

At large sample-to-detector distances (more than about 10 m), the scattering from water is not sufficiently strong to enable its use for correcting sample scattering curves obtained with the same settings. Experience shows that it is possible in this case to use a water scattering curve measured at a shorter sample-to-detector distance. This should be sufficiently large not to be influenced by the deviation of the (flat) detector surface from the spherical shape of the scattered waves and small enough so that the scattering intensity per detector element is still sufficient, for example about 3 m. It is necessary to know the intensity loss factor due to the different solid angles covered by the detector element and by the apparent source in both cases. This can be determined, for instance, by comparing the global scattering intensity of water on the whole detector for both conditions (after correction for the background scattering) or from the intensity shift of the same sample measured at both detector distances in a plot of the logarithm of the intensity *versus* Q.

2.6.2.6.3. *Estimation of the incoherent scattering level*

For an exact knowledge of the scattering curve, it is necessary to subtract the level of incoherent scattering from the scattering curve, which is initially a superposition of the (desired) coherent sample scattering, electronic and neutron background noise, and (sometimes dominant) incoherent scattering.

A frequently used technique is the subtraction of a reference sample that has the same level of incoherent scattering, but lacks the coherent scattering from the inhomogeneities under study. Although this seems simple in the case of solutions, in practice there are problems: Very often, the $^1H/^2H$ mixture is made by dialysis, and the last dialysis solution is taken as the reference. The dialysis has to be excessive to obtain really identical levels of ^1H, and in reality there is often a disagreement that is more important the lower the sample concentration is. If the concentration is high, then the incoherent scattering from the sample atoms (protons) themselves becomes important.

For dilute aqueous solutions, there is a procedure using the sample and reference transmissions for estimating the incoherent background level (May, Ibel & Haas, 1982): The incoherent scattering level from the sample, $I_{i,s}$, can be estimated as

$$I_{i,s} = I[H_2O]f_\lambda(1 - T_s)/(1 - T[H_2O]), \qquad (2.6.2.9)$$

where $I[H_2O]$ is the scattering from a water sample, $T[H_2O]$ is transmission, T_s that of the sample. f_λ is a factor depending on the wavelength, the detector sensibility, the solvent composition, and the sample thickness; it can be determined experimentally by plotting $I_{i,s}/I[H_2O]$ *versus* $(1 - T_s)/(1 - T[H_2O])$ for a number of partially deuterated solvent mixtures.

This procedure is justified because of the overwhelming contribution of the incoherent scattering of ^1H to the macroscopic scattering cross section of the solution, and therefore to its transmission. The procedure should also be valid for organic solvents. The precision of the estimation is limited by the precision of the transmission measurement, the relative error of which can hardly be much better than about 0.005 for reasonable measuring times and currently available equipment, and by the (usually small) contribution of the coherent cross section to the total cross section of the solution. A modified version of (2.6.2.9) can be used if a solvent with a transmission close to that of a sample has been measured, but the factor f_λ should not be omitted.

An equation similar to (2.6.2.9) holds for systems with a larger volume occupation c of particles in a (protonated) solvent with a scattering level I_{inc} in a cell with identical pathway (without the particles):

$$I_{i,s} = I_{inc}(1 - T_{inc}^{1-c})/(1 - T_{inc}). \qquad (2.6.2.9a)$$

In this approximation, the particles' cross-section contribution is assumed to be zero, *i.e.* the particles are considered as bubbles.

In the case of dilute systems of monodisperse particles, the residual background (after initial corrections) can be quite well estimated from the zero-distance value of the distance-distribution function calculated by the indirect Fourier transformation of Glatter (1979).

2.6.2.6.4. *Inner surface area*

According to Porod (1951, 1982), small-angle scattering curves behave asymptotically like $I(Q) = \text{constant} \times A_sQ^{-4}$ for large Q, where A_s is the inner surface of the sample. Theoretically, fitting a straight line to $I(Q)Q^4$ *versus* Q^4 ('Porod plot') *at sufficiently large* Q therefore yields a zero intercept, which is proportional to the internal surface; a slope

can be interpreted as a residual constant background (including the self-term of the constant nuclear 'form factor'), which may be used for slightly correcting the estimated background and consequently improving the quality of the data. For monodispersed particles, a particle surface can be deduced from the overall surface. The value of the surface area so determined depends on the maximal Q to which the scattering curve can be obtained with good statistics. This depends also on the magnitude of the background. At least for weakly scattering particles in mixtures of ^1H_2O and ^2H_2O, and even more in pure ^1H_2O, the incoherent background level often cannot be determined precisely enough for interpreting the tail of the scattering curve in terms of the surface area.

2.6.2.7. *Single-particle scattering*

Single-particle scattering in this context means scattering from isolated structures (clusters in alloys, isolated polymer chains in a solvent, biological macromolecules, *etc*.) randomly distributed in space and sufficiently far away from each other so that interparticle contributions to the scattering (see Subsection 2.6.2.8) can be neglected. The tendency of polymerization of single particles, for example the monomer–dimer equilibrium of proteins or the formation of higher aggregates, and long-range (*e.g.* electrostatic) interactions between the particles disturb single-particle scattering. In the absence of such effects, samples with solute volume fractions below about 1% can be regarded as free of volume-exclusion interparticle effects for most purposes. For (monodispersed) protein samples, for example, this means that concentrations of about $5\,\mathrm{mg\,ml^{-1}}$ are often a good compromise between sufficient scattering intensity and concentration effects. In many cases, series of scattering measurements with increasing particle concentrations have been used for extrapolating the scattering to zero concentration. In the following, we assume that particle interactions are absent.

2.6.2.7.1. *Particle shape*

All X-ray and neutron small-angle scattering curves can be approximated by a parabolic fit in a narrow Q range near $Q = 0$ (Porod, 1951): $I(Q) \simeq I(0)\ (1 - a^2Q^2/3 + \ldots)$. In the case of single-particle scattering, a Gaussian approximation to the scattering curve is even more precise (Guinier & Fournet, 1955) in the zero-angle limit:

$$I(Q) \simeq I(0)\exp(-Q^2/3R_G^2), \qquad (2.6.2.10)$$

where R_G is the radius of gyration of the particle's excess scattering density.

The concept of R_G and the validity of the Guinier approximation is discussed in more detail in the SAXS section of this volume (§2.6.1). It might be mentioned here that the frequently used $QR_G < 1$ rule for the validity of the Guinier approximation is no more than an indication and should always be tested by a scattering calculation with the model obtained from the experiment: Spheres yield a deviation of 5% of the Gaussian approximation at $QR_G = 1.3$, rods at $QR_G = 0.6$; ellipsoids of revolution with an elongation factor of 2 can reach as far as $QR_G = 3$.

More detailed shape information requires a wider Q range. As indicated before, Fourier transforms may help to distinguish between conflicting models. In many instances (*e.g.* hollow bodies, cylinders), it is much easier to find the shape of the scattering particle from the distance distribution function than from the scattering curve [see §2.6.2.7.3].

2.6.2.7.2. *Particle mass*

With $N = CN_AV_s/M_r$, where N_A is Avogadro's number, C is the mass concentration of the solute in $\mathrm{g\,l^{-1}}$, and V_s is the sample volume in $\mathrm{cm^{-3}}$ (we assume N identical particles randomly distributed in dilute solution), we find that the relative molecular mass M_r of a particle can be determined from the intensity at zero angle, $I(0)$ in equation (2.6.2.10), using the relation (Jacrot & Zaccai, 1981), where the particle mass concentration C (in $\mathrm{mg\,ml^{-1}}$) is omitted:

$$I(0)/\{CI[\mathrm{H_2O}](0)\} = 4\pi f\, T_sM_rN_Ad_s\, 10^{-3}\left[\left(\sum b_i - \rho_sV\right)/M_r\right]^2/(1 - T[\mathrm{H_2O}]). \qquad (2.6.2.11)$$

d_s is the sample thickness. Note that $\sum b_i/M_r$ may depend on solvent exchange; in a given solvent, especially ^1H_2O, it is rather independent of the exact amino acid composition of proteins (Jacrot & Zaccai, 1981).

An alternative presentation of equation (2.6.2.11) is

$$I(0)/\{CI[\mathrm{H_2O}](0)\} = 4\pi f\, T_sM_rd_s\ 10^{-3}(v\Delta\rho)^2/N_A(1 - T[\mathrm{H_2O}]), \qquad (2.6.2.11a)$$

where $\Delta\rho = \rho_p(\rho_s) - \rho_s$ is the contrast; ρ_p is the particle scattering-length density (depending on the scattering-length density ρ_s of the solvent, in general) and v is the partial specific volume of the particle. Expression (2.6.2.11*a*) is of advantage when $(v\Delta\rho)$, which is a linear function of ρ_s, is known for a class of particles.

A thermodynamic approach to the particle-size problem, in view of the complementarity of different methods, has been given Zaccai, Wachtel & Eisenberg (1986) on the basis of the theory of Eisenberg (1981). It permits the determination of the molecular mass, of the hydration, and of the amount of bound salts.

2.6.2.7.3. *Real-space considerations*

The scattering from a large number of randomly oriented particles at infinite dilution, and as a first approximation that of particles at sufficiently high dilution (see above), is completely determined by a function $p(r)$ in real space, the distance-distribution function. It describes the probability p of finding a given distance r between any two volume elements within the particle, weighted with the product of the scattering-length densities of the two volume elements.

Theoretically, $p(r)$ can be obtained by an infinite sine Fourier transform of the isolated-particle scattering curve

$$I(Q) = \int_0^\infty [p(r)/Qr]\sin(Qr)\,\mathrm{d}r. \qquad (2.6.2.12)$$

In practice, the scattering curve can be measured neither to $Q = 0$ (but an extrapolation is possible to this limit), nor to $Q \to \infty$. In fact, neutrons allow us to measure more easily the sample scattering in the range near $Q = 0$; X-rays are superior for large Q values. Indirect iterative methods have been developed that fit the finite Fourier transform

$$I(Q) = \int_0^{D_{\max}} [p(r)/Qr]\sin(Qr)\,\mathrm{d}r \qquad (2.6.2.12a)$$

of a $p(r)$ function described by a limited number of parameters between $r = 0$ and a maximal chord length $D_{\max}$ within the particle to the experimental scattering curve. It differs from the $p(r)$ of Section 2.6.1 by a factor of 4π.

This procedure was termed the 'indirect Fourier transformation (IFT)' method by Glatter (1979), who uses equidistant B splines in real space that are correlated by a Lagrange parameter, thus reducing the number of independent parameters to be fitted. Errors in determining a residual flat background only affect the innermost spline at $r = 0$; the intensity at $Q = 0$ and the radius of gyration are not influenced by a (small) flat background.

Another IFT method was introduced by Moore (1980), who uses an orthogonal set of sine functions in real space. This procedure is more sensitive to the correct choice of $D_{\max}$ and to a residual background that might be present in the data.

A major advantage of IFT is the ease with which the deconvolution of the scattering intensities with respect to the wavelength distribution and to geometrical smearing due to the primary beam and sample sizes is calculated by smearing the theoretical scattering curve obtained from the real-space model. In fact, it is possible to convolute the scattering curves obtained from the single splines that are calculated only once at the beginning of the fit procedure. The convoluted constituent curves are then iteratively fitted to the experimental scattering curves.

With the exception of particle symmetry, which is better seen in the scattering curve, structural features are more easily recognized in the $p(r)$ function (Glatter, 1982*a*).

Once the $p(r)$ function is determined, the zero-angle intensity and the radius of gyration can be calculated from its integral and from its second moment, respectively.

2.6.2.7.4. *Particle-size distribution*

Indirect Fourier transformation also facilitates the evaluation of particle-size distributions on the assumption that all particles have the same shape and that the size distribution depends on only one parameter (Glatter, 1980).

2.6.2.7.5. *Model fitting*

As in small-angle X-ray scattering, the scattering curves can be compared with those of simple or more elaborate models. This is rather straightforward in the case of highly symmetric particles like icosahedral viruses that can be regarded as spherical at low resolution. The scattering curves of such viruses are easily adapted by spherical-shell models assigning different scattering-length densities to the different shells (*e.g.* Cusack, 1984). Neutron constrast variation helps decisively to distinguish between the shells.

Fitting complicated models to the scattering curves is more critical because of the averaging effect of small-angle scattering. While it is correct and easy to show that the scattering curve produced by a model body coincides with the measured curve, in general a unique model cannot be deduced from the scattering curve alone. Stuhrmann (1970) has presented a procedure using Lagrange polynomials to calculate low-resolution real-space models directly from the scattering information. It has been applied successfully to the scattering curves from ribosomes (Stuhrmann *et al.*, 1976).

2.6.2.7.6. *Label triangulation*

Triangulation is one of the techniques that make full use of the advantages of neutron scattering. It consists in specifically labelling single components of a multicomponent complex, measuring the scattering curves from (*a*) particles with two labelled components, (*b*) and (*c*) particles with either of the two components labelled, and (*d*) a (reference) particle that is not labelled at all. The comparison of the scattering from $(b) + (c)$ with that from $(a) + (d)$ yields information on the scattering originating exclusively from vectors combining volume elements in one component with volume elements in the other component.

From this scattering difference curve, the distances between the centres of mass of the components are obtained. A table of such distances yields the spatial arrangement of the components. If there are n components in the complex, at least $4n - 10$ for $n > 3$ distance values are needed to build this model: Three distances define a basic triangle, three more yield a basic tetrahedron, the handedness of which is arbitrary and has to be determined by independent means. At least four more distances are required to fix a further component in space. More than four distances are needed if the resulting tetrahedron is too flat.

Label triangulation is based on a technique developed by Kratky & Worthmann (1947) for determining heavy-metal distances in organometallic compounds by X-ray scattering, and was proposed originally by Hoppe (1972); Engelman & Moore (1972) first saw the advantage of neutrons. The need to mix preparations (*a*) plus (*d*) and (*b*) plus (*c*) for obtaining the desired scattering difference curve in the case of high concentrations and/or inhomogeneous complexes (consisting of different classes of matter) has been shown by Hoppe (1973). The complete map of all protein positions within the small subunit from *E. coli* ribosomes has been obtained with this method (Capel *et al.*, 1987). An alternative approach for obtaining the distance information contained in the scattering curves from pairs of proteins by fitting the Fourier transform of 'moving splines' to the scattering curves has been presented by May & Nowotny (1989) for data on the large ribosomal subunit.

The scattering curves should be measured at the scattering-length-density matching point of the reference particle for reducing undesired contributions. Naturally inhomogeneous particles can be rendered homogeneous by specific partial deuteration. This technique has been successfully applied for ribosomes (Nierhaus *et al.*, 1983).

2.6.2.7.7. *Triple isotropic replacement*

An elegant way of determining the structure of a component inside a molecular complex has been proposed by Pavlov & Serdyuk (1987). It is based on measuring the scattering curves from three preparations. Two contain the complex to be studied at two different levels of labelling, ρ_1 and ρ_2, and are mixed together to yield sample 1, the third contains the complex at an intermediate level of labelling, ρ_3 (sample 2). If the condition

$$\rho_3(\mathbf{r}) = (1 - \delta)\rho_1(\mathbf{r}) + \delta\rho_2(\mathbf{r}) \qquad (2.6.2.13)$$

is satisfied by δ, the relative concentration of particle 2 in sample 1, then the difference between the scattering from the two samples only contains contributions from the single component. Additionally, the contributions from contamination, aggregation, and interparticle effects are suppressed provided that they are the same in the three samples, *i.e.* independent of the partial-deuteration states.

In the case of small complexes, δ can be obtained by measuring the scattering curves $I_1(Q)$, $I_2(Q)$, and $I_3(Q)$ of the three particles as a function of contrast and by plotting the differences of the zero-angle scattering $I_1(0) - I_3(0)$ and $I_2(0) - I_3(0)$ *versus* δ. The two curves intercept at the correct ratio δ_0.

The method, which can be considered as a special case of a systematic inverse contrast variation of a selected component, holds if the concentrations, the complex occupations, and the aggregation behaviour of the three particles are identical. Mathematically, the difference curve is independent of the

contrast of the rest of the complex with respect to the solvent. In practice, it would be wise to follow the same considerations as with triangulation.

2.6.2.8. *Dense systems*

Especially in the case of polymers, but also in alloys, the scattering from the sample can often no longer be described, as in the previous section, as originating from a sum of isolated particles in different orientations. There may be two reasons for this: either the number concentration c of one of the components is higher than about 0.01, leading to excluded-volume effects, and/or there is an electrostatic interaction between components (for example, in solutions of polyelectrolytes, latex, or micelles). In these cases, it is usually the information about the *structure* of the sample caused by the interactions that is to be obtained rather than the shape of the inhomogeneities or particles in the sample, unless the interactions can be regarded as a weak disturbance.

An excellent introduction to the treatment of dense systems is found in the article of Hayter (1985). A detailed description of the theoretical interpretation of correlations in charged macromolecular and supramolecular solutions has been published by Chen, Sheu, Kalus & Hoffmann (1988).

The scattering from densely packed particles can be written as the product of the structure factor or structure function $S(Q)$, describing the arrangement of the inhomogeneities with respect to each other, in mathematical terms the interference effects of correlations between particle positions, in the sample,

$$S(Q) = \left\langle \sum \sum \exp[i\mathbf{Q}(\mathbf{r}_j - \mathbf{r}_k)] \right\rangle / N, \tag{2.6.2.14}$$

and of the form factor $P(Q)$ of the inhomogeneities (as before):

$$I(Q) = P(Q)S(Q). \tag{2.6.2.15}$$

Hayter & Penfold (1981) were the first to describe an analytic structure factor for macro-ion solutions.

If $P(Q)$ can be obtained from a measurement of a dilute solution of the particles under study, then the pure structure factor can be calculated by dividing the high-concentration intensity curve by the low-concentration curve. This procedure requires the form factor not to change with concentration, which is not necessarily the case for loosely arranged particles such as polymers. A technique that avoids this problem is contrast variation (see Subsection 2.6.2.2): introducing a fraction of a deuterated molecule into a bulk of identical protonated molecules (or *vice versa*, with the advantage of reduced incoherent background) yields the scattering of the 'isolated' labelled particle at high-concentration conditions.

Partial structure factors can be obtained from a contrast-variation series of a given system at different volume fractions of the particles. Similarly to equation (2.6.2.4), the structure factor can be decomposed into a quadratic function. In the ternary alloy Al–Ag–Zn, for example, the scattering has been decomposed into the contributions from the two minor species Ag and Zn, and their interference, *i.e.* the partial structure functions for Zn–Zn, Zn–Ag, and Ag–Ag, by using the scattering from three samples with different silver isotopes, and identical sample treatment (Salva-Ghilarducci, Simon, Guyot & Ansara, 1983).

2.5.1 (*cont.*)

Giessen, B. C. & Gordon, G. E. (1968). *X-ray diffraction: new high-speed technique based on X-ray spectroscopy*. *Science*, **159**, 973–975.

Glazer, A. M., Hidaka, M. & Bordas, J. (1978). *Energy-dispersive powder profile refinement using synchrotron radiation*. *J. Appl. Cryst.* **11**, 165–172.

Häusermann, D. (1992). *New techniques for new sources: a fresh look at energy-dispersive diffraction for high-pressure studies*. *High Press. Res.* **8**, 647–654.

Holzapfel, W. B. & May, W. (1982). *Improvements in energy dispersive X-ray diffraction with conical slit and diamond cell. High-pressure research in geophysics*, edited by S. Akimoto & M. H. Manghnani, pp. 73–80, and references therein. Dordrecht: Reidel.

Kalman, Z. H. (1979). *On the derivation of integrated reflected energy formulae*. *Acta Cryst.* A**35**, 634–641.

Laine, E. & Lähteenmäki, I. (1980). *The energy-dispersive X-ray diffraction method*: *annotated bibliography 1968–78*. *J. Mater. Sci.* **15**, 269–278, and references therein.

Mao, H. K., Jephcoat, A. P., Hemley, R. J., Finger, L. W., Zha, C. S., Hazen, R. M. & Cox, D. E. (1988). *Synchrotron X-ray diffraction measurements of single crystal hydrogen to 26.5 GigaPascals*. *Science*, **239**, 1131–1134.

Nelmes, R. J. & McMahon, M. I. (1994). *High-pressure powder diffraction on synchrotron sources*. *J. Synchrotron Rad.* **1**, 69–73.

Neuling, H. W. & Holzapfel, W. B. (1992). *Rietveld analysis for energy dispersive X-ray diffraction under high pressure with synchrotron radiation*. *High Press. Res.* **8**, 665–660.

Olsen, J. S. (1992). *Instrumentation for high-pressure X-ray diffraction research at HASYLAB*. *Rev. Sci. Instrum.* **63**, 1058–1061.

Olsen, J. S., Buras, B., Jensen, T., Alstrup, O., Gerward, L. & Selsmark, B. (1978). *Influence of polarization of the incident beam on integrated intensities in X-ray energy-dispersive diffractometry*. *Acta Cryst.* A**34**, 84–87.

Otto, J. W. (1997). *A facility for high-pressure X-ray diffraction at HASYLAB*. *Nucl. Instrum. Methods*, A**384**, 552–557.

Parrish, W. & Hart, M. (1987). *Advantages of synchrotron radiation for polycrystalline diffractometry*. *Z. Kristallogr.* **179**, 161–173.

Ruoff, A. L. (1992). *EDXD studies above 400 GPa (and prospects for obtaining pressures near 1 TPa and doing EDXD studies at such pressures)*. *High Press. Res.* **8**, 639–645.

Uno, R. & Ishigaki, A. (1975). *The correction of experimental structure factors for thermal diffuse scattering in white X-ray diffraction*. *Jpn. J. Appl. Phys.* **14**, 291–292.

Wilson, A. J. C. (1973). *Note on the aberrations of a fixed-angle energy-dispersive powder diffractometer*. *J. Appl. Cryst.* **6**, 230–237.

2.5.2

Buras, B. & Gerward, L. (1975). *Relations between integrated intensities in crystal diffraction methods for X-rays and neutrons*. *Acta Cryst.* A**31**, 372–374.

Buras, B. & Leciejewicz, J. (1964). *A new method for neutron diffraction crystal structure investigations*. *Phys. Status Solidi*, **4**, 349–355.

Buras, B., Mikke, K., Lebech, B. & Leciejewicz, J. (1965). *The time-of-flight method for investigations of single-crystal structures*. *Phys. Status Solidi*, **11**, 567–573.

Jauch, W., Schultz, A. J. & Schneider, J. R. (1988). *Accuracy of single crystal time-of-flight neutron diffraction: a comparative study of MnF_2*. *J. Appl. Cryst.* **21**, 975–979.

Johnson, M. W. & David, W. I. F. (1985). *HPRD: the high resolution powder diffractometer at the spallation neutron source*. Report RAL-85-112. Rutherford Appleton Laboratory, Chilton, Didcot, Oxon, UK.

Jorgensen, J. D. & Rotella, F. J. (1982). *High-resolution time-of-flight powder diffractometer at the ZING-P′ pulsed neutron source*. *J. Appl. Cryst.* **15**, 27–34.

Jorgensen, J. D. & Worlton, T. G. (1985). *Disordered structure of D_2O ice VII from in situ neutron powder diffraction*. *J. Chem. Phys.* **83**, 329–333.

Lowde, R. D. (1956). *A new rationale of structure-factor measurement in neutron-diffraction analysis*. *Acta Cryst.* **9**, 151–155.

Marmeggi, J. C. & Delapalme, A. (1980). *Neutron Laue photographs of crystallographic satellite reflections in alpha-uranium*. *Physica (Utrecht)*, **102**B, 309–312.

Schultz, A. J., Srinivasan, K., Teller, R. G., Williams, J. M. & Lukehart, C. M. (1984). *Single-crystal time-of-flight neutron diffraction structure of hydrogen cis-diacetyltetracarbonylrhenate*. *J. Am. Chem. Soc.* **106**, 999–1003.

Steichele, E. & Arnold, P. (1975). *A high-resolution neutron time-of-flight diffractometer*. *Phys. Lett.* A**44**, 165–166.

Turberfield, K. C. (1970). *Time-of-flight neutron diffractometry*. *Thermal neutron diffraction*, edited by B. T. M. Willis, pp. 34–50. Oxford University Press.

Windsor, C. G. (1981). *Pulsed neutron diffraction*. London: Taylor & Francis.

2.6.1

Anderegg, J. W., Beeman, W. W., Shulman, S. & Kaesberg, P. J. (1955). *An investigation of the size, shape and hydration of serum albumin by small-angle X-ray scattering J. Am. Chem. Soc.* **77**, 2927–2937.

Bayvel, L. P. & Jones, A. R. (1981). *Electromagnetic scattering and its applications*. London: Applied Science Publishers.

Bonse, U. & Hart, M. (1965). *An X-ray interferometer*. *Appl. Phys. Lett.* **6**, 155–156.

Bonse, U. & Hart, M. (1966). *An X-ray interferometer*. *Z. Phys.* **189**, 151–156.

Bonse, U. & Hart, M. (1967). In *Small-angle X-ray scattering,* edited by H. Brumberger. New York: Gordon and Breach.

Bracewell, R. (1986). *Fourier transform and its applications*. New York: McGraw-Hill.

Brumberger, H. (1967). *Small-angle X-ray scattering*. New York: Gordon and Breach.

Chen, S. H., Sheu, E. Y., Kalus, J. & Hoffmann, H. (1988). *Small-angle neutron scattering investigation of correlations in charged macromolecular and supramolecular solutions*. *J. Appl. Cryst.* **21**, 751–769.

Cleemann, J. C. & Kratky, O. (1960). *Größe, Gestalt und Solvatation des Edestinmoleküls aus dem Studium der Röntgenkleinwinkelstreuung*. *Z. Naturforsch. Teil B*, **15**, 525–535.

Damaschun, G., Damaschun, H., Müller, J. J., Ruckpaul, K. & Zinke, M. (1974). *Vergleich der Struktur von Proteinen im Kristall und in Lösung; Theoretische und experimentelle Untersuchungen mittels der Röntgen-Klein-winkelstreuung am Hämoglobin*. *Stud. Biophys.* **47**, 27–39.

2.6.1 (*cont.*)

Damaschun, G., Gernat, C., Damaschun, H., Bychkova, V. E. & Ptitsyn, O. B. (1986). *Comparison of intramolecular packing of a protein in native and 'molten globule' states*. *Int. J. Biol. Macromol.* **8**, 226–230.

Damaschun, G. & Pürschel, H. V. (1971*a*). *Röntgen-Kleinwinkelstreuug von isotropen Proben ohne Fernordnung. I. Allgemeine Theorie*. *Acta Cryst.* A**27**, 193–197.

Damaschun, G. & Pürschel, H. V. (1971*b*). *Berechnung von Streumassenradien aus unverschmierten und spaltverschmierten Röntgen-Kleinwinkelstreukurven*. *Monatsh. Chem.* **102**, 1146–1155.

Debye, P. (1915). *Zerstreuung von Röntgenstrahlen*. *Ann. Phys. (Leipzig)*, **46**, 809–823.

Debye, P. & Bueche, A. M. (1949). *Scattering by an inhomogeneous solid*. *J. Appl. Phys.* **20**, 518–525.

Debye, P. & Menke, H. (1930). *Bestimmung der inneren Struktur von Flüssigkeiten mit Röntgenstrahlen*. *Phys. Z.* **31**, 797–798.

Fedorov, B. A. & Denesyuk, A. I. (1978). *Large-angle X-ray diffuse scattering, a new method for investigating changes in the conformation of globular proteins in solution*. *J. Appl. Cryst.* **11**, 473–477.

Fedorov, B. A., Ptitsyn, O. B. & Voronin, L. A. (1972). *X-ray diffuse scattering of globular protein solutions: consideration of the solvent influence*. *FEBS Lett.* **28**, 188–190.

Fedorov, B. A., Ptitsyn, O. B. & Voronin, L. A. (1974*a*). *Small-angle X-ray scattering of native hog thyroglobulin*. *J. Appl. Cryst.* **7**, 181.

Fedorov, B. A., Ptitsyn, O. B. & Voronin, L. A. (1974*b*). *X-ray diffuse scattering by polypeptides and proteins in solution. IV. Consideration of the solvent effect for globular protein solutions*. *Mol. Biol. (Moscow)*, **8**, 693–709.

Feigin, L. A. & Svergun, D. I. (1987). *Structure analysis by small-angle X-ray and neutron scattering*. New York: Plenum.

Gernat, C., Damaschun, G., Kröber, R., Bychkova, V. E. & Ptitsyn, O. B. (1986). *Large-angle diffuse X-ray scattering from a homopolypeptide and some proteins*. *Stud. Biophys.* **112**, 213–219.

Glatter, O. (1972). *X-ray small angle scattering of molecules composed of subunits*. *Acta Phys. Austriaca*, **36**, 307–315.

Glatter, O. (1977*a*). *Data evaluation in small-angle scattering: calculation of the radial electron density distribution by means of indirect Fourier transformation*. *Acta Phys. Austriaca,* **47**, 83–102.

Glatter, O. (1977*b*). *A new method for the evaluation of small-angle scattering data*. *J. Appl. Cryst.* **10**, 415–421.

Glatter, O. (1979). *The interpretation of real-space information from small-angle scattering experiments*. *J. Appl. Cryst.* **12**, 166–175.

Glatter, O. (1980*a*). *Evaluation of small-angle scattering data from lamellar and cylindrical particles by the indirect transformation method*. *J. Appl. Cryst.* **13**, 577–584.

Glatter, O. (1980*b*). *Determination of particle-size distribution functions from small-angle scattering data by means of the indirect transformation method*. *J. Appl. Cryst.* **13**, 7–11.

Glatter, O. (1980*c*). *Computation of distance distribution functions and scattering functions of models for small-angle scattering experiments*. *Acta Phys. Austriaca*, **52**, 243–256.

Glatter, O. (1981). *Convolution square root of band-limited symmetrical functions and its application to small-angle scattering data*. *J. Appl. Cryst.* **14**, 101–108.

Glatter, O. (1982*a*). In *Small angle X-ray scattering,* edited by O. Glatter & O. Kratky, Chap. 4. London: Academic Press.

Glatter, O. (1982*b*). In *Small angle X-ray scattering*, edited by O. Glatter & O. Kratky, Chap. 5. London: Academic Press.

Glatter, O. (1988). *Comparison of two different methods for direct structure analysis from small-angle scattering data*. *J. Appl. Cryst.* **21**, 886–890.

Glatter, O. & Hainisch, B. (1984). *Improvements in real-space deconvolution of small-angle scattering data*. *J. Appl. Cryst.* **17**, 435–441.

Glatter, O. & Hofer, M. (1988*a*). *Interpretation of elastic light-scattering data in real space. II. Nonspherical and inhomogeneous monodisperse systems*. *J. Colloid Interface Sci.* **112**, 484–495.

Glatter, O. & Hofer, M. (1988*b*). *Interpretation of elastic light-scattering data. III. Determination of size distributions of polydisperse systems*. *J. Colloid Interface Sci.* **122**, 496–506.

Glatter, O., Hofer, M., Jorde, C. & Eigner, W.-D. (1985). *Interpretation of elastic light-scattering data in real space*. *J. Colloid Interface Sci.* **105**, 577–586.

Glatter, O. & Kratky, O. (1982). *Small angle X-ray scattering*. London: Academic Press.

Goodisman, J. (1980). *The correlation function, intersect distribution and scattering from a cube*. *J. Appl. Cryst.* **13**, 132–134.

Greville, T. N. E. (1969). *Theory and applications of spline functions*. New York: Academic Press.

Guinier, A. (1939). *La diffraction des rayons X aux très petits angles: application à l'étude de phénomènes ultramicroscopiques*. *Ann. Phys. (Paris)*, **12**, 161–237.

Guinier, A. & Fournet, G. (1955). *Small angle scattering of X-rays*. New York: John Wiley.

Heidorn, D. B. & Trewhella, J. (1988). *Comparison of the crystal and solution structures of calmodulin and troponin C*. *Biochemistry*, **27**, 909–915.

Heine, S., Kratky, O. & Roppert, J. (1962). *Lichstreuung und Röntgenkleinwinkelstreuung von statistisch verknäuelter. Fadenmolekülen, berechnet nach der Monte Carlo Methode*. *Makromol. Chem.* **56**, 150–168.

Hendricks, R. W. (1978). *The ORNL 10-meter small-angle X-ray scattering camera*. *J. Appl. Cryst.* **11**, 15–30.

Hendrix, J. (1985). *Position-sensitive X-ray detectors*. *Adv. Polym. Sci.* **67**, 59–98.

Hofer, M., Schurz, J. & Glatter, O. (1989). *Oil–water emulsions: particle size distributions from elastic light-scattering data*. *J. Colloid Interface Sci.* **127**, 147–155.

Holmes, K. C. (1982). In *Small angle X-ray scattering,* edited by O. Glatter & O. Kratky, Chap. 3.II. London: Academic Press.

Hosemann, R. & Bagchi, S. N. (1952). *Existenzbeweis für eine eindeutige Röntgenstrukturanalyse durch Entfaltung. I. Entfaltung zentrosymmetrischer endlicher Massenverteilungen*. *Acta Cryst.* **5**, 749–762.

Hosemann, R. & Bagchi, S. N. (1962). *Direct analysis of diffraction by matter*. Amsterdam: North-Holland.

Hubbard, S. T., Hodgson, K. O. & Doniach, S. (1988). *Small-angle X-ray scattering investigation of the solution structure of troponin C*. *J. Biol Chem.* **263**, 4151–4158.

I'anson, K. J., Bacon, J. R., Lambert, N., Miles, M. J., Morris, V. J., Wright, D. J. & Nave, C. (1987). *Synchrotron radiation wide-angle X-ray scattering of glycinin solutions*. *Int. J. Biol. Macromol.* **9**, 368–370.

Kirste, R. G. & Oberthür, R. C. (1982). In *Small angle X-ray scattering*, edited by O. Glatter & O. Kratky, Chap. 12. London: Academic Press.

Koch, M. H. J. (1988). *Instruments and methods for small-angle scattering with synchrotron radiation*. *Macromol. Symp.* **15**, 79–90.

2.6.1 (*cont.*)

Kratky, O. (1982*a*). In *Small angle X-ray scattering*, edited by O. Glatter & O. Kratky, Chap. 3.I. London: Academic Press.

Kratky, O. (1982*b*). In *Small angle X-ray scattering,* edited by O. Glatter & O. Kratky, Chap. 11. London: Academic Press.

Kratky, O. & Leopold, H. (1970). *A comparison between Bonse–Hart and the block collimation system. Makromol. Chem.* **133**, 181–195.

Kratky, O. & Porod, G. (1948). *Die Abhängigkeit der Röntgen-Kleinwinkelstreuung von Form und Größe der kolloider Teilchen in verdünnten Systemen. III. Acta Phys. Austriaca*, **2**, 133–147.

Kratky, O. & Porod, G. (1949). *Röntgenuntersuchung gelöster Fadenmoleküle. Recl Trav. Chim. Pays-Bas*, **68**, 1106–1122.

Kratky, O. & Porod, G. (1953). In *Die Physik der Hochpolymere*, Vol. II, edited by H. A. Stuart. Berlin: Springer.

Kratky, O., Porod, G. & Kahovec, L. (1951). *Einige Neuerungen in der Technik und Auswertung von Röntgen-Kleinwinkelmessungen. Z. Elektrochem.* **55**, 53–59.

Kratky, O. & Worthmann, W. (1947). *Über die Bestimmbarkeit der Konfiguration gelöster organischer Moleküle durch interferometrische Vermessung mit Röntgenstrahlen. Monatsh. Chem.* **76**, 263–281.

Krigbaum, W. R. & Kügler, F. R. (1970). *Molecular conformation of egg-white lysozyme and bovine-lactalbumin in solution. Biochemistry*, **9**, 1216–1223.

Laggner, P. (1982). In *Small-angle X-ray scattering*, edited by O. Glatter & O. Kratky, Chap. 10. London: Academic Press.

Langridge, R., Marvin, D. A., Seeds, W. E., Wilson, H. R., Cooper, C. W., Wilkins, M. H. F. & Hamilton, L. D. (1960). *The molecular configuration of deoxyribonucleic acid. J. Mol. Biol.* **2**, 38–62.

Leopold, H. (1982). In *Small-angle X-ray scattering,* edited by O. Glatter & O. Kratky, Chap. 3.III. London: Academic Press.

Luzzati, V. (1960). *Interprétation des mesures absolues de diffusion centrale des rayons X en collimation ponctuelle ou linéaire: solutions de particules globulaires et de batonnets. Acta Cryst.* **13**, 939–945.

Mittelbach, P. (1964). *Zur Röntgenkleinwinkelstreuung verdünnter kolloider Systeme. VIII. Acta Phys. Austriaca*, **19**, 53–102.

Mittelbach, P. & Porod, G. (1961*a*). *Zur Röntgenkleinwinkelstreuung verdünnter kolloider Systeme. Die Berechnung der Streukurven von Parallelepipeden. Acta Phys. Austriaca*, **14**, 185–211.

Mittelbach, P. & Porod, G. (1961*b*). *Zur Röntgenkleinwinkelstreuung verdünnter kolloider Systeme. VI. Acta Phys. Austriaca*, **14**, 405.

Mittelbach, P. & Porod, G. (1962). *Zur Röntgenkleinwinkelstreuung verdünnter kolloider Systeme. VII. Die Berechnung der Streukurven von dreiachsigen Ellipsoiden. Acta Phys. Austriaca,* **15**, 122–147.

Mittelbach, P. & Porod, G. (1965). *Zur Röntgenkleinwinkelstreuung verdünnter kolloider Systeme. Kolloid Z. Z. Polym.* **202**, 40–49.

Moore, P. B. (1980). *Small-angle scattering. Information content and error analysis. J. Appl. Cryst.* **13**, 168–175.

Müller, J. J., Damaschun, G., Damaschun, H., Misselwitz, R., Zirwer, D. & Nothnagel, A. (1984). *X-ray scattering evidence that calf thymus DNA in solution is a double helix and not a warped zipper. Biomed. Biochim. Acta*, **43**, 929–936.

Müller, J. J., Damaschun, G. & Schrauber, H. (1990). *The highly resolved excess electron distance distribution of biopolymers in solution – calculation from intermediate-angle X-ray scattering and interpretation. J. Appl. Cryst.* **23**, 26–34.

Müller, K. & Glatter, O. (1982). *Practical aspects of the use of indirect Fourier transformation methods. Makromol. Chem.* **183**, 465–479.

Ninio, J. & Luzzati, V. (1972). *Comparative small-angle X-ray scattering studies on unacylated, acylated and cross-linked Escherichia coli transfer* RNA_1^{Val}. *J. Mol. Biol.* **71**, 217–229.

Pessen, H., Kumosinski, T. F. & Timasheff, S. N. (1973). *Small-angle X-ray scattering. Methods Enzymol.* **27**, 151–209.

Pilz, I. (1982). In *Small-angle X-ray scattering,* edited by O. Glatter & O. Kratky, Chap. 8. London: Academic Press.

Pilz, I., Glatter, O. & Kratky, O. (1980). *Small-angle X-ray scattering. Methods Enzymol.* **61**, 148–249.

Pilz, I., Glatter, O., Kratky, O. & Moring-Claesson, O. (1972). *Rötgenkleinwinkelstudien über die Substruktur von Helix pomatia Hämocyanin. Z. Naturforsch. Teil B*, **27**, 518.

Pilz, I., Goral, K., Hoylaerts, M., Witters, R. & Lontie, R. (1980). *Studies by small-angle X-ray scattering of the quaternary structure of the 24-S component of the haemocyanin of Astacus leptodactylus in solution. Eur. J. Biochem.* **105**, 539–543.

Porod, G. (1948). *Die Abhängigkeit der Röntgen-Kleinwinkelstreuung von Form und Größe der kolloiden Teilchen in verdünnten Systemen. IV. Acta Phys. Austriaca*, **2**, 255–292.

Porod, G. (1949). *Zusammenhang zwischen mittlerem Endpunktsabstand und Kettenlänge bei Fadenmolekülen. Monatsh. Chem.* **80**, 251–255.

Porod, G. (1951). *Die Röntgenkleinwinkelstreuung von dichtgepackten kolloiden Systemen. I. Kolloid Z.* **124**, 83–114.

Porod, G. (1952). *Die Röntgenkleinwinkelstreuung von dichtgepackten kolloiden Systemen. II. Kolloid Z.* **125**, 51–122.

Porod, G. (1982). In *Small-angle X-ray scattering*, edited by O. Glatter & O. Kratky, Chap. 2. London: Academic Press.

Ritland, H. N., Kaesberg, P. & Beeman, W. W. (1950). *Double crystal and slit methods in small angle X-ray scattering. J. Appl. Phys.* **21**, 838–841.

Ruckpaul, K., Damaschun, G., Damaschun, H., Dimitrov, D. P., Jänig, G. R., Müller, J. J., Pürschel, H.-V. & Behlke, J. (1973). *Der Einfluß verschiedener Pufferionen auf die Funktion und Struktur von adultem menschlichen Hämoglobin. Acta Biol. Med. Germ.* **31**, 679–690.

Sadler, D. M. & Worcester, D. L. (1982). *Neutron diffraction studies of oriented photosynthetic membranes. J. Mol. Biol.* **159**, 467–484.

Schelten, J. & Hossfeld, F. (1971). *Application of spline functions to the correction of resolution errors in small-angle scattering. J. Appl. Cryst.* **4**, 210–223.

Shannon, C. E. & Weaver, W. (1949). *The mathematical theory of communication*. Urbana: University of Illinois Press.

Stasiecki, P. & Stuhrmann, H. B. (1978). *Röntgenkleinstwinkelstreuung an Erythrocyten. J. Appl. Cryst.* **11**, 1–5.

Stuhrmann, H. B. (1970*a*). *Interpretation of small-angle scattering functions of dilute solutions and gases. A representation of the structures related to a one-particle-scattering function. Acta Cryst.* A**26**, 297–306.

Stuhrmann, H. B. (1970*b*). *Ein neus Verfahren zur Bestimmung der Oberflächenform und der inneren Struktur von gelösten globulären Proteinen aus Röntgenkleinwinkelmessungen. Z. Phys. Chem.* **72**, 177–184.

2.6.1 (*cont.*)

Stuhrmann, H. B. (1970*c*). *Die Bestimmung der Oberflächenform von gelöstem Myoglobin aus Röntgenkleinwinkelmessungen. Z. Phys. Chem.* **72**, 185–198.

Stuhrmann, H. B. (1978). *The use of X-ray synchrotron radiation for structural research in biology. Rev. Biophys.* **11**, 71–98.

Stuhrmann, H. B. (1982). In *Small-angle X-ray scattering,* edited by O. Glatter & O. Kratky, Chap. 6. London: Academic Press.

Stuhrmann, H. B., Koch, M. H. J., Parfait, J., Haas, J., Ibel, K. & Crichton, R. R. (1977). *Shape of the 50S subunit of Escherichia coli ribosomes. Proc. Natl Acad. Sci. USA*, **74**, 2316–2320.

Svergun, D. I., Feigin, L. A. & Schedrin, B. M. (1982). *Small-angle scattering: direct structure analysis. Acta Cryst.* A**38**, 827–835.

Svergun, D. I., Feigin, L. A. & Schedrin, B. M. (1984). *The solution of the one-dimensional sign problem for Fourier transforms. Acta Cryst.* A**40**, 137–142.

Tikhonov, A. N. & Arsenin, V. Ya. (1977). *Solution of ill-posed problems:* New York: John Wiley.

Walter, G., Kranold, R. & Becherer, G. (1974). *Zu Problemen der Ver- und Entschmierung von Röntgen-Kleinwinkel-Streukurven. Stud. Biophys.* **47**, 49–62.

Zernicke, F. & Prins, J. A. (1927). *Die Beugung von Röntgenstrahlen in Flüssigkeiten als Effekt der Molekülanordnung. Z. Phys.* **41**, 184–194.

Zipper, P. (1969). *Ein einfaches Verfahren zur Monochromatisierung von Streukurven. Acta Phys. Austriaca*, **30**, 143–151.

2.6.2

Abragam, A., Bacchella, C. L., Coustham, J., Glättli, H., Fourmond, M., Malinowski, A., Meriel, P., Pinot, M. & Roubeau, A. (1982). *The interest in spin dependent nuclear scattering amplitudes. J. Phys. (Paris)*, **43**(C7), 373–381.

Alefeld, B., Schwahn, D. & Springer, T. (1989). *New developments of small angle neutron scattering instruments with focusing. Nucl. Instrum. Methods*, A**274**, 210–216.

Bacon, G. E. (1975). *Neutron diffraction.* Oxford: Clarendon Press.

Benoit, H. & Wippler, C. (1960). *Répartition angulaire de la lumière diffusée par une solution de copolymères. J. Chim. Phys.* **57**, 524–527.

Bonse, M. & Hart, M. (1966). *Small-angle X-ray scattering by spherical particles of polystyrene and polyvinyltoluene. Z. Phys.* **189**, 151–162.

Boothroyd, A. T. (1989). *The effect of gravity on the resolution of small-angle neutron scattering. J. Appl. Cryst.* **22**, 252–255.

Bragg, W. L. & Perutz, M. F. (1952). *The external form of the haemoglobin molecule. I. Acta Cryst.* **5**, 277–283.

Capel, M. S., Engelman, D. M., Freeborn, B. R., Kjeldgaard, M., Langer, J. A., Ramakrishnan, V., Schindler, D. G., Schneider, D. K., Schoenborn, B. P., Sillers, I.-Y., Yabuki, S. & Moore, P. B. (1987). *A complete mapping of the proteins in the small ribosomal subunit of Escherichia coli. Science*, **238**, 1403–1406.

Chen, S. H., Sheu, E. Y., Kalus, J. & Hoffmann, H. (1988). *Small-angle neutron scattering investigation of correlations in charged macromolecular and supramolecular solutions. J. Appl. Cryst.* **21**, 751–769.

Cusack, S. (1984). *Neutron scattering studies of virus structure. Neutrons in biology; basic life sciences,* Vol. 27, edited by B. P. Schoenborn, pp. 173–188. New York: Plenum.

Cusack, S., Mellema, J. E., Krijgsman, P. C. J. & Miller, A. (1981). *An investigation of the structure of alfalfa mosaic virus by small-angle neutron scattering. J. Mol. Biol.* **145**, 525–543.

Eisenberg, H. (1981). *Forward scattering of light, X-rays and neutrons. Q. Rev. Biophys.* **14**, 141–172.

Engelman, D. M. & Moore, P. B. (1972). *A new method for the determination of biological quaternary structure by neutron scattering. Proc. Natl Acad. Sci. USA,* **69**, 1997–1999.

Glatter, O. (1979). *The interpretation of real-space information from small-angle scattering experiments. J. Appl. Cryst.* **12**, 166–175.

Glatter, O. (1980). *Determination of particle-size distribution functions from small-angle scattering data by means of the indirect transformation method. J. Appl. Cryst.* **13**, 7–11.

Glatter, O. (1982*a*). *Interpretation. Small-angle X-ray scattering*, edited by O. Glatter & O. Kratky, pp. 167–196. London: Academic Press.

Glatter, O. (1982*b*). *Data treatment. Small-angle X-ray scattering*, edited by O. Glatter & O. Kratky, pp. 119–165. London: Academic Press.

Glatter, O. & Kratky, O. (1982). Editors. *Small-angle X-ray scattering*. London: Academic Press.

Guinier, A. (1968). *Small-angle scattering. International Tables for X-ray crystallography*, Vol. III, 2nd ed., edited by C. H. Macgillavry & G. D. Rieck, pp. 324–329. Birmingham: Kynoch Press.

Guinier, A. & Fournet, G. (1955). Editors. *Small-angle scattering of X-rays*. New York: John Wiley.

Hayter, J. B. (1985). *Determination of the structure and dynamics of micellar solutions by neutron small-angle scattering. Physics of amphiphiles: micelles, vesicles and micro-emulsions,* edited by V. Degiorgio & M. Corti, pp. 59–93. Amsterdam: North-Holland.

Hayter, J. B. & Penfold, J. (1981). *An analytic structure factor for macro-ion solutions. Mol. Phys.* **42**, 109–118.

Hjelm, R. P. (1988). *The resolution of TOF low-Q diffractometers: instrumental, data acquisition and reduction factors. J. Appl. Cryst.* **21**, 618–628.

Hoppe, W. (1972). *A new X-ray method for the determination of the quaternary structure of protein complexes. Isr. J. Chem.* **10**, 321–333.

Hoppe, W. (1973). *The 'label triangulation' method and the 'mixed isomorphous replacement' principle. J. Mol. Biol.* **78**, 581–585.

Ibel, K. (1976). *The neutron small-angle camera D11 at the high-flux reactor, Grenoble. J. Appl. Cryst.* **9**, 296–309.

Ibel, K. & Stuhrmann, H. B. (1975). *Comparison of neutron and X-ray scattering of dilute myoglobin solutions. J. Mol. Biol.* **93**, 255–265.

Jacrot, B. (1976). *The study of biological structures by neutron scattering from solution. Rep. Prog. Phys.* **10**, 911–953.

Jacrot, B. & Zaccai, G. (1981). *Determination of molecular weight by neutron scattering. Biopolymers*, **20**, 2413–2426.

Janot, C. & George, B. (1985). *Surface states and magnetic heterogeneity in iron-based glasses. J. Phys. (Paris) Lett.* **46**, L85–L88.

Knoll, W., Schmidt, K. & Ibel, K. (1985). *The inverse contrast variation in small-angle neutron scattering: a sensitive technique for the evaluation of lipid phase diagrams. J. Appl. Cryst.* **18**, 65–70.

2.6.2 (*cont.*)

Knop, W., Nierhaus, K. H., Nowotny, V., Niinikoski, T. O., Krumpolc, M., Rieubland, J. M., Rijlart, A., Schärpf, O., Schink, H.-J., Stuhrmann, H. B. & Wagner, R. (1986). *Polarised neutron scattering from dynamic polarised targets of biological origin*. *Helv. Phys. Acta*, **59**, 741–746.

Kostorz, G. (1979). *Small-angle scattering and its applications to materials science*. *Treatise on materials science and technology,* Vol. 15, edited by G. Kostorz, pp. 227–289. New York: Academic Press.

Kostorz, G. (1988). *Small-angle neutron scattering – metallurgical applications*. *Materials science forum,* Vols. 27/28, edited by M. M. Elcombe & T. J. Hicks, pp. 325–344. Aedermannsdorf, Switzerland: Trans Tech Publications.

Kratky, O. & Worthmann, W. (1947). *Über die Bestimmbarkeit der Konfiguration gelöster organischer Moleküle durch interferometrische Vermessung mit Röntgenstrahlen*. *Monatsh. Chem.* **76**, 263–281.

Lindner, P., May, R. P. & Timmins, P. A. (1992). *Upgrading the SANS instrument D11 at the ILL*. *Physica (Utrecht)*, B**180–181**, 967–972.

Lindner, P. & Oberthür, R. C. (1985). *Shear induced deformation of polystyrene coils in dilute solution from small angle neutron scattering. 1. Shear gradient apparatus and first results*. *Colloid Polym. Sci.* **263**, 443–453.

Lindner, P. & Oberthür, R. C. (1988). *Shear-induced deformation of polystyrene coils in dilute solution from small angle neutron scattering. 2. Variation of shear gradient, molecular mass and solvent viscosity*. *Colloid Polym. Sci.,* **263**, 443–453.

Luzzati, V., Tardieu, A., Mateu, L. & Stuhrmann, H. B. (1976). *Structure of human serum lipoprotein in solution. I. Theory and techniques of an X-ray scattering approach using solvents of variable density*. *J. Mol. Biol.* **101**, 115–127.

May, R. P., Ibel, K. & Haas, J. (1982). *The forward scattering of cold neutrons by mixtures of light and heavy water*. *J. Appl. Cryst.* **15**, 15–19.

May, R. P. & Nowotny, V. (1989). *Distance information derived from neutron low-Q scattering*. *J. Appl. Cryst.* **22**, 231–237.

Moore, P. B. (1980). *Small-angle scattering. Information content and error analysis*. *J. Appl. Cryst.* **13**, 168–175.

Nierhaus, K. H., Lietzke, R., May, R. P., Nowotny, V., Schulze, H., Simpson, K., Wurmbach, P. & Stuhrmann, H. B. (1983). *Shape determination of ribosomal proteins in situ*. *Proc. Natl Acad. Sci. USA*, **80**, 2889–2893.

Pavlov, M. Yu. & Serdyuk, I. N. (1987). *Three-isotropic substitutions method in small-angle neutron scattering*. *J. Appl. Cryst.* **20**, 105–110.

Pedersen, J. S., Posselt, D. & Mortensen, K. (1990). *Analytical treatment of the resolution function for small-angle scattering*. *J. Appl. Cryst.* **23**, 321–333.

Porod, G. (1951). *Die Röntgenkleinwinkelstreuung von dichtgepackten kolloiden Systemen*. *Kolloid Z.* **124**, 83–114.

Porod, G. (1982). *General theory*. *Small-angle X-ray scattering,* edited by O. Glatter & O. Kratky, pp. 17–51. London: Academic Press.

Salva-Ghilarducci, A., Simon, J. P., Guyot, P. & Ansara, I. (1983). *Precipitation in ternary Al–Zn–Ag alloys studied by isotropic contrast in neutron small angle scattering*. *Acta Metall.* **31**, 1705–1713.

Schelten, J. & Hossfeld, F. (1971). *Application of spline functions to the correction of resolution errors in small-angle scattering*. *J. Appl. Cryst.* **4**, 210–223.

Stuhrmann, H. B. (1970). *Interpretation of small-angle scattering functions of dilute solutions and gases. A representation of the structures related to a one-particle-scattering function*. *Acta Cryst.* A**26**, 297–306.

Stuhrmann, H. B., Haas, J., Ibel, K., de Wolf, B., Koch, M. H. J., Parfait, R. & Crichton, R. R. (1976). *New low resolution model for 50S subunit of Escherichia coli ribosomes*. *Proc. Natl Acad. Sci. USA*, **73**, 2379–2383.

Stuhrmann, H. B. & Kirste, R. G. (1965). *Elimination der intrapartikulären Untergrundstreuung bei der Röntgenkleinwinkelstreuung an kompakten Teilchen (Proteinen)*. *Z. Phys. Chem. Neue Folge,* **46**, 247–250.

Stuhrmann, H. B., Schärpf, O., Krumpolc, M., Niinikoski, T. O., Rieubland, M. & Rijllart, A. (1986). *Dynamic nuclear polarisation of nuclear matter*. *Eur. Biophys. J.* **14**, 1–6.

Timmins, P. A. & Zaccai, G. (1988). *Low resolution structures of biological complexes studied by neutron scattering*. *Eur. Biophys. J.* **15**, 257–268.

Wignall, G. D. (1987). *Neutron scattering*. *Encyclopedia of polymer science and engineering,* Vol. 10, 2nd ed., edited by J. I. Kroschwitz, pp. 112–184. New York: John Wiley.

Wignall, G. D. & Bates, F. S. (1987). *Absolute calibration of small-angle neutron scattering data*. *J. Appl. Cryst.* **20**, 28–40.

Wignall, G. D., Christen, D. K. & Ramakrishnan, V. (1988). *Instrumental resolution effects in small-angle neutron scattering*. *J. Appl. Cryst.* **21**, 438–451.

Witz, J. (1983). *Contrast variation of the small-angle neutron scattering of globular particles: the influence of hydrogen exchange*. *Acta Cryst.* A**39**, 706–711.

Zaccai, G. & Jacrot, B. (1983). *Small angle neutron scattering*. *Annu. Rev. Biophys. Bioeng.* **12**, 139–157.

Zaccai, G., Wachtel, E. & Eisenberg, H. (1986). *Solution structure of halophilic malate dehydrogenase from small-angle neutron and X-ray scattering and ultracentrifugation*. *J. Mol. Biol.* **190**, 97–106.

2.7

Allinson, N. M. (1994). *Development of non-intensified charge-coupled device area X-ray detectors*. *J. Synchrotron Rad.* **1**, 54–62.

Allinson, N. M., Allsopp, D. W. E., Quayle, J. A. & Magorrian, B. G. (1991). *Effects of soft X-ray irradiation on solid-state imagers*. *Nucl. Instrum. Methods*, A**310**, 267–272.

Armstrong, R. W. & Wu, C. C. (1973) *X-ray diffraction microscopy*. *Tools and techniques for microstructural analysis*, edited by J. L. McCall & W. M. Mueller, pp. 169–219. New York: Plenum.

Arndt, U. W. (1986). *X-ray position-sensitive detectors*. *J. Appl. Cryst.* **19**, 145–163.

Arndt, U. W. (1990). *X-ray television area detectors*. *Synchrotron Radiat. News*, **3**, 17–22.

Authier, A. (1961). *Etude de la transmission anormale des rayons X dans des cristaux de silicium. I. Case des cristaux parfaits*. *Bull. Soc. Fr. Minéral. Cristallogr.* **84**, 51–89.